Phonons in low-dimensional systems

2004 J. Phys.: Condens. Matter 16 S395

(http://iopscience.iop.org/0953-8984/16/5/005)

INSTITUTE OF PHYSICS PUBLISHING JOURNAL OF PHYSICS: CONDENSED MATTER

J. Phys.: Condens. Matter **16** (2004) S395–S427 PII: S0953-8984(04)66833-0

Phonons in low-dimensional systems

A P Mayer, D Bonart and D Strauch

Institute for Theoretical Physics, University of Regensburg, D-93040 Regensburg, Germany

Received 25 July 2003
Published 23 January 2004
Online at stacks.iop.org/JPhysCM/16/S395 (DOI: 10.1088/0953-8984/16/5/005)

Abstract

An introduction is given to the dynamical properties of crystalline systems having lattice-translational symmetry in less than three dimensions. These include surfaces of and interfaces between crystals, layered structures (2D lattice periodicity), bars and wires (1D lattice periodicity), as well as crystallites and clusters that have no lattice translational symmetry at all. In addition, superlattices are covered as artificial materials, giving rise to interesting dynamical effects. Crystal surfaces and crystalline bars are considered in some detail. For these systems, changes of the atomic equilibrium positions in comparison to the corresponding bulk crystals are also discussed since they frequently affect the dynamical properties.

1. Introduction

The dynamical properties of structures with reduced lattice-translational symmetry are a fascinating topic to study since they give rise to various interesting phenomena. They are relevant for a number of electronic processes in semiconductor heterostructures, for thermal properties, in particular thermal transport properties of such systems, for stability considerations of nanostructures, etc, and hence they are partly of technological importance, too. In the following discussions, we shall mainly focus on phenomena, but we shall also introduce a few theoretical methods that will enable us to determine quantitatively vibrational properties of these structures and partly lead to a qualitative understanding. Experimental techniques for the investigation of atomic vibrations in the systems considered will not be discussed. They would require a review on their own. In the following theoretical considerations, we shall not go beyond the harmonic approximation and we shall always assume the existence of a lattice potential or force constants. Modern methods of computing these force constants have partly been the subject of an earlier lecture at this school and are reviewed in [1].

On the basis of continuum theory derived for the long-wavelength acoustic and long-wavelength optical regime, a number of phonon modes in systems with planar geometries will be discussed. Subsequently effects will be treated that are beyond the realm of continuum theory, in particular relaxation and reconstruction of bare and adsorbate-covered surfaces.

As an example system with 1D lattice translational invariance the relaxation and dynamical properties of diatomic bars with square cross sections will be studied in some detail. Finally, a method will be presented that allows for an efficient computation of partial densities of states without requiring lattice periodicity.

2. General considerations

In the following, we shall label the atoms that our systems consist of by the index l and denote their equilibrium positions by $\mathbf{X}(l)$. The actual position of atom l is $\mathbf{R}(l) = \mathbf{X}(l) + \mathbf{u}(l)$ with the displacement vector $\mathbf{u}(l)$.

Within the harmonic approximation, the lattice potential energy $\Phi(\{\mathbf{R}(l)\})$ is expanded to second order in the displacements

$$\Phi(\{\mathbf{R}(l)\}) = \Phi_0 + \tfrac{1}{2}\sum_{l,l'}\sum_{\alpha,\beta}\Phi_{\alpha\beta}(ll')u_\alpha(l)u_\beta(l'), \tag{2.1}$$

which leads to the following equations of motion for the Cartesian components of the displacement vectors:

$$m_l\ddot{u}_\alpha(l) = -\sum_{l',\beta}\Phi_{\alpha\beta}(ll')u_\beta(l'). \tag{2.2}$$

In 3D crystals, the index l is decomposed into ℓ, labelling the unit cell, and κ, numbering the sublattices. One may decompose $\mathbf{X}(l) = \mathbf{X}(\ell) + \mathbf{X}(\kappa)$, where $\mathbf{X}(\ell)$ is the position of the ℓth unit cell and $\mathbf{X}(\kappa)$ the position of the atom belonging to sublattice κ with the origin placed in the position of this unit cell.

ℓ may be regarded as a composite index, $\ell = (\ell_1, \ell_2, \ell_3)$ with integers ℓ_1, ℓ_2, ℓ_3 being the prefactors of the basic translation vectors in their linear combination that is equal to $\mathbf{X}(\ell)$.

The displacements $\mathbf{u}(\ell\kappa)$ may be decomposed into normal modes

$$u_\alpha(\ell\kappa) = \sum_{\mathbf{q}j}\frac{e_\alpha(\kappa|\mathbf{q}j)}{\sqrt{m_\kappa}}\mathrm{e}^{\mathrm{i}\mathbf{q}\cdot\mathbf{X}(\ell)}Q(\mathbf{q}j). \tag{2.3}$$

Here, $\mathbf{q}$ is a wavevector in the three-dimensional Brillouin zone, j labels the $3n$ phonon branches, where n is the number of sublattices, and $(e_\alpha(\kappa|\mathbf{q}j))$ is an eigenvector of the dynamical matrix $\mathbf{D}$:

$$\omega^2_{\mathbf{q}j}e_\alpha(\kappa|\mathbf{q}j) = \sum_{\beta,\kappa'}D_{\alpha\beta}(\mathbf{q}|\kappa\kappa')e_\beta(\kappa'|\mathbf{q}j), \tag{2.4}$$

$$D_{\alpha\beta}(\mathbf{q}|\kappa\kappa') = \frac{1}{\sqrt{m_\kappa m_{\kappa'}}}\sum_{\ell'}\Phi\begin{pmatrix}0 & \ell'\\ \kappa & \kappa'\end{pmatrix}\mathrm{e}^{\mathrm{i}\mathbf{q}\cdot\mathbf{X}(\ell')}. \tag{2.5}$$

The phonon frequencies $\omega_{\mathbf{q}j}$ are usually presented for wavevectors along the main symmetry directions of the Brillouin zone (figure 1).

In a semi-infinite crystal, the lattice translational symmetry is lost along the direction normal to the surface, but is preserved in the directions parallel to the surface. As a consequence, the unit cell of this structure is infinitely extended into the depth (figure 2). The index l may again be decomposed into a cell index ℓ and an index κ labelling the (infinitely many) sublattices, i.e. the layers and the atoms per layer belonging to a unit cell. The displacements may again be decomposed into normal modes according to (2.3), where $\mathbf{q}$ is now a two-dimensional wavevector in the 2D surface Brillouin zone, and $j = 1, 2, \ldots, \infty$ labels the branches.

The various vibrational modes of a semi-infinite crystal may be classified as:

- bulk modes: the eigenvector $(e_\alpha(\kappa|\mathbf{q}j))$ is non-zero at arbitrarily large distance from the surface,

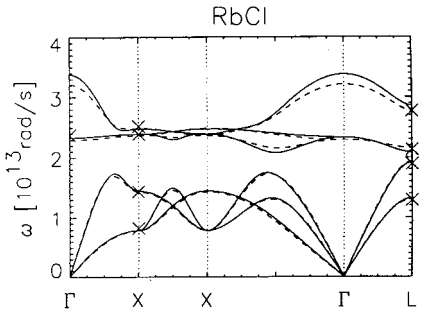

Figure 1. Phonon dispersion curves of RbCl. Model calculations, full: [2], broken: [3]. Experimental data (crosses) taken from [4].

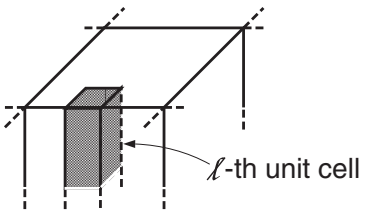

Figure 2. Semi-infinite crystal and unit cell, shown schematically.

- surface modes: the eigenvector is localized at or near the surface,
- surface resonances: the eigenvector is mostly localized at the surface, but does not vanish in the limit of infinite depth.

In practical calculations, the problem of broken lattice-translational symmetry at the surface is dealt with in two ways:

(1) The Green function method, which treats the surface as a defect [5, 6]. This method is rarely used nowadays, but can be useful when dealing with surface modes of large penetration depth.
(2) The slab method [7], in nowadays' *ab initio* calculations especially the method of 'repeated slabs' [8]. The 3D lattice periodicity is restored when—instead of a semi-infinite crystal—a slab of finite thickness is considered and this slab is repeated periodically an infinite number of times (figure 3). Care has to be taken that the thickness of the slab is sufficiently large that surface modes on both sides of the slab do not interact. This would give rise to spurious frequency splittings. Also, the distance between adjacent slabs has to be large enough for the modes in neighbouring slabs not to interact. The infinite periodic stack of slabs may be treated as a 3D crystal, and only those 3D wavevectors have to be considered that are parallel to the layers.

When plotting the phonon dispersion relation of the slab system for wavevectors along symmetry directions in the surface Brillouin zone, a number of branches are obtained that increase with increasing slab thickness. These branches—often called 'spaghetti'—fill up bands that become continuous in the limit of infinite slab thickness. These bands correspond to bulk phonon modes whose 3D dispersion relation is projected on the surface Brillouin zone in a manner illustrated in figure 4. The frequencies of all bulk phonon modes with 3D wavevectors $\mathbf{q}_{3D} = (q_1, q_2, q_3)^T$ and any value of q_3 such that $\mathbf{q}_{3D}$ is in the 3D Brillouin zone

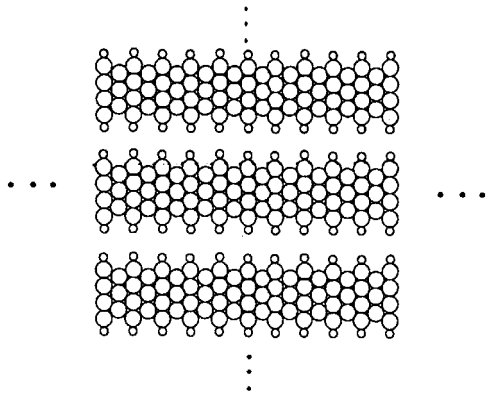

Figure 3. Repeated slab geometry, shown schematically (from [9]).

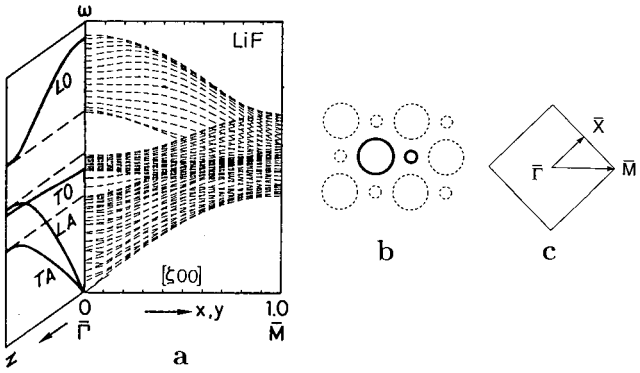

Figure 4. Bulk projected dispersion relation of a (100) surface of LiF (a) (from [7]). Top view of the surface with unit cell (b) and surface Brillouin zone (c) (from [2]).

of the crystal are plotted at the 2D wavevector $\mathbf{q}_{2D} = (q_1, q_2)^T$. This presentation of the bulk phonon frequencies is called 'surface adapted'.

In addition to the bulk bands, isolated branches may appear in gaps between the bulk bands and below the acoustic band. They correspond to surface phonon modes.

The same general considerations apply to semi-infinite crystals with a number of adsorbate layers on their surfaces.

Crystal bars and wires of infinite length, but finite cross section, exhibit lattice translational symmetry along their axis (the z axis). The index l is again decomposed in ℓ and κ, where ℓ labels the unit cells along the z axis and κ the atoms in a unit cell. The number n of atoms per unit cell increases with increasing cross-sectional area. An example for a unit cell of a bar made of an alkali halide with (100) surfaces is shown in figure 5. In the decomposition of the displacements in normal modes, the wavevector is now one-dimensional in a 1D Brillouin zone.

The dispersion relation of the phonon modes of such a bar consists of $3n$ branches. With $n \to \infty$, these branches form bands. In the example of a diatomic bar shown in figure 6, there is a gap between the bands of acoustic and optical bulk mode frequencies. In this gap, a band of surface modes is situated. In addition to these bands, isolated branches are found that correspond to modes localized at the edges of the bar.

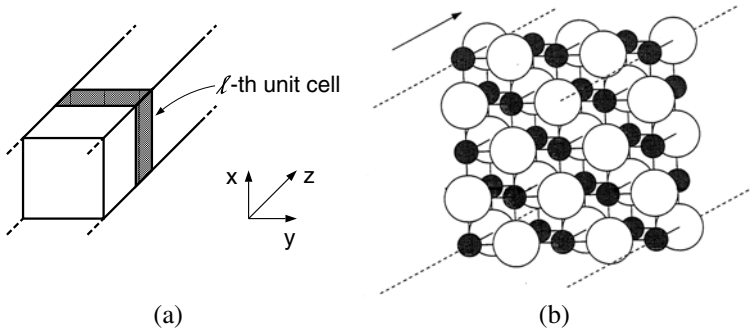

Figure 5. Infinite crystal bar and unit cell, shown schematically (upper panel). Unit cell of an alkali halide bar with quadratic cross section and (001) surfaces (from [10]) (lower panel).

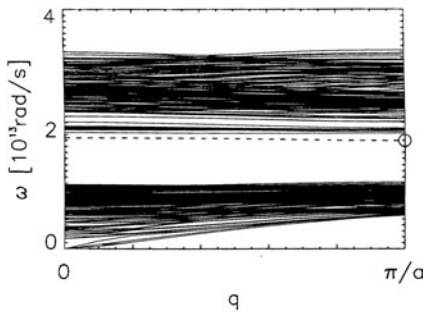

Figure 6. Phonon dispersion relation of a crystalline bar with 9×9 atoms per cross-sectional layer. The broken line corresponds to edge-localized modes (from [11]).

In finite isolated structures like crystal cubes, for example, no wavevector of the normal modes can reasonably be defined. If the cube consists of N atoms, there will be $3N$ normal modes. For large numbers of N, their frequencies cluster in bands corresponding to bulk modes, surface modes and edge modes. In addition, there may be isolated frequencies corresponding to modes with vibrational amplitudes localized at the corners of the cube (see, e.g., [12]).

In most practical cases (e.g. in various types of semiconductor nanostructures), wires, cubes, pyramids, etc, are embedded in substrates or grown on a substrate, or they form more complicated heterostructure geometries. In such hybrid systems, interface modes and edge modes involving more than one material have to be expected.

3. Continuum theory

For wavelengths long compared to the nearest-neighbour spacing of the underlying lattice, certain phonon modes in 3D bulk crystals as well as in dimensionally reduced structures can be determined within a continuum approach. Application of continuum theory to lattice-dynamical systems is useful for various reasons. It is helpful in interpreting and testing lattice-dynamical calculations and gaining a basic understanding of certain vibrational modes. In addition, resonant interaction of free carriers in semiconductor crystals and heterostructures are normally with longitudinal long-wavelength optical phonons and long-wavelength acoustic phonons. For a quantitative determination of the frequencies and displacement patterns of these

phonon modes within continuum theory, only a few material constants are required that are tabulated (see, for example, [13]). For quantitatively reliable lattice-dynamical calculations, much greater efforts would be needed.

Before proceeding with applications, we first give a short derivation of the field equations of continuum theory from lattice dynamics. For this purpose, we start with the Lagrangian L for a crystal including a macroscopic electric field $\mathbf{E}$ that is treated in the quasi-static approximation which is justified in the frequency regime of phonon modes:

$$L = \sum_{\ell,\kappa,\alpha} \tfrac{1}{2} m_\kappa \dot{u}_\alpha(\ell\kappa)\dot{u}_\alpha(\ell\kappa) - \Phi(\{R_\alpha(\ell\kappa)\}) + \sum_{\ell,\kappa,\alpha,\beta} Z_{\alpha|\beta}(\kappa) u_\beta(\ell\kappa) E_\alpha(\mathbf{X}(\ell\kappa)) + \int \mathrm{d}^3X \sum_{\alpha,\beta} \tfrac{1}{2}\varepsilon^{(\infty)}_{\alpha\beta} E_\alpha(\mathbf{X}) E_\alpha(\mathbf{X}). \tag{3.1}$$

The coupling between the atomic displacements and the macroscopic electric field is treated within the dipole approximation. In (3.1), $Z_{\alpha|\beta}(\kappa)$ are the components of the tensor of Born effective charges (or the first-order dipole coefficients), and $\varepsilon^{(\infty)}_{\alpha\beta}$ are the components of the high-frequency dielectric tensor of the crystal. The part of the electric field fluctuating on short scales is contained in the potential energy Φ.

We now perform a linear transformation of the atomic displacement variables $u_\alpha(\ell\kappa)$ to new variables that contain the displacements of the centres of mass of the unit cells, $U_\alpha(\ell)$, and relative displacements $Y_\alpha(\ell\lambda)$ ([14]). In order to simplify the following derivations, we shall consider diatomic crystals only, where $Y_\alpha(\ell) = u_\alpha(\ell 1) - u_\alpha(\ell 2)$. A generalization to crystals with more than two atoms per unit cell is largely straightforward. We now assume that the values of $Y_\alpha(\ell)$ and $U_\alpha(\ell)$ vary little when moving from unit cell ℓ to a unit cell ℓ' in the neighbourhood. One may then introduce continuous fields $\mathbf{Y}(\mathbf{X})$ and $\mathbf{U}(\mathbf{X})$. $\mathbf{U}$ is the displacement field, while $Z\mathbf{Y}$ is the dynamic part of the crystal's polarization. For simplicity, we assume here further symmetries of the crystal that are present in GaAs, for example, and which imply that the tensor of Born effective charges reduces to one charge Z and the dielectric tensor to one dielectric constant ε_∞.

The macroscopic electric field is expressed as a negative gradient of a scalar potential ϕ. Up to second order in all variables, the Lagrangian then takes the form

$$L = \int \mathrm{d}^3X \left\{ \tfrac{1}{2}\rho \dot{U}_\alpha(\mathbf{X})\dot{U}_\alpha(\mathbf{X}) + \tfrac{1}{2} m_\mathrm{R} \dot{Y}_\alpha(\mathbf{X})\dot{Y}_\alpha(\mathbf{X}) - \tilde{\Phi}(\{U_{\alpha,\beta}(\mathbf{X}), Y_\alpha(\mathbf{X})\}) - Z Y_\alpha(\mathbf{X})\phi_{,\alpha}(\mathbf{X}) + \frac{\varepsilon_\infty}{2}\phi_{,\alpha}(\mathbf{X})\phi_{,\alpha}(\mathbf{X}) \right\} \tag{3.2}$$

with density of potential energy

$$\tilde{\Phi} = \tfrac{1}{2}\bar{C}_{\alpha\beta\mu\nu} U_{\alpha,\beta} U_{\mu,\nu} + G_{\alpha\beta|\gamma} U_{\alpha,\beta} Y_\gamma + \tfrac{1}{2} m_\mathrm{R} \omega_0^2 Y_\alpha Y_\alpha. \tag{3.3}$$

In (3.2), (3.3) and the following equations, we use the short-hand index notation $\ldots_{,\alpha}$ for the partial derivative $\partial \ldots / \partial X_\alpha$, and we invoke the summation convention for Cartesian indices (summation over repeated Cartesian indices is implied). For reasons of convenience, we shall frequently use the lower-case letters x, y, z for the three components of the vector $\mathbf{X}$ instead of X_1, X_2, X_3. (Since we are restricting our considerations to linear theory, a distinction between material and spatial coordinates need not be made here.) For the last term of (3.3) we have again assumed the appropriate symmetry of the crystal. m_R is the reduced mass and ω_0 the TO frequency at the Brillouin zone centre. The Lagrangian (3.2) with (3.3) contains material constants specific to a certain homogeneous crystal. In heterostructures, these material constants are functions of the spatial coordinate $\mathbf{X}$.

Applying Hamilton's principle, the following field equations follow from (3.2):

$$\rho\ddot{U}_\alpha = \frac{\partial}{\partial X_\beta}\{\bar{C}_{\alpha\beta\mu\nu}U_{\mu,\nu} + G_{\alpha\beta|\gamma}Y_\gamma\}, \tag{3.4}$$

$$m_{\mathrm{R}}\{\ddot{Y}_\alpha + \omega_0^2 Y_\alpha\} = -G_{\mu\nu|\alpha}U_{\mu,\nu} - Z\phi_{,\alpha}, \tag{3.5}$$

$$\frac{\partial}{\partial X_\alpha}\{-\varepsilon_\infty\phi_{,\alpha} + ZY_\alpha\} = 0. \tag{3.6}$$

Equation (3.6) is Poisson's equation. At surfaces and interfaces, the material constants have jumps, and boundary conditions have to be imposed on the fields. These boundary conditions follow partly from the Lagrangian (3.2), too. Due to the discontinuities of material constants, variation of the Lagrangian with respect to the field variables produces Dirac delta functions. The requirement that the prefactors of these delta functions have to vanish plays the role of boundary conditions.

Since we have confined ourselves to linear theory, the time dependence of the field variables may be chosen to be $\propto \exp(-\mathrm{i}\omega t)$. We now discuss separately the frequency regimes of long-wavelength acoustic and optical phonons.

3.1. Regime of long-wavelength acoustic phonons

Since $\omega \ll \omega_0$ in this regime, we may neglect the second time derivative in (3.5) and eliminate $\mathbf{Y}$ from (3.4) and (3.6), $Y_\alpha \approx (-1/m_{\mathrm{R}}\omega_0^2)\{G_{\mu\nu|\alpha}U_{\mu,\nu} + Z\phi_{,\alpha}\}$, to arrive at two coupled equations for the displacement field and the electrostatic potential:

$$\rho\ddot{U}_\alpha = \frac{\partial}{\partial X_\beta}\sigma_{\alpha\beta} \tag{3.7}$$

with stress tensor components

$$\sigma_{\alpha\beta} = C_{\alpha\beta\mu\nu}U_{\mu,\nu} + e_{\alpha\beta\nu}\phi_{,\nu}, \tag{3.8}$$

and

$$D_{\alpha,\alpha} = 0 \tag{3.9}$$

with the following expression for the components of the dielectric displacement $\mathbf{D}$:

$$D_\alpha = -\varepsilon_0\phi_{,\alpha} + e_{\mu\nu\alpha}U_{\mu,\nu}. \tag{3.10}$$

Here, $C_{\alpha\beta\mu\nu}$ are the elastic moduli of the crystal that may differ from $\bar{C}_{\alpha\beta\mu\nu}$ by contributions resulting from internal strains (sublattice displacements in response to homogeneous strains). $e_{\alpha\beta\gamma}$ are the piezoelectric constants and ε_0 is the static dielectric constant.

In addition to the field equations, boundary conditions apply at free surfaces and at interfaces between two different media. These are the continuity of the components of the displacement field, U_α, the electrostatic potential ϕ, the normal component of the dielectric displacement, $\hat{N}_\alpha D_\alpha$, and of the quantities $\hat{N}_\beta\sigma_{\alpha\beta}$ at interfaces. At free surfaces, $\hat{N}_\beta\sigma_{\alpha\beta}$ has to vanish. (Here $\hat{\mathbf{N}}$ is a unit vector normal to the interface/surface.)

3.2. Regime of long-wavelength optical phonons

Now $\omega \approx \omega_0$. We again solve (3.5) for $\mathbf{Y}$:

$$Y_\alpha = \frac{Z}{m_{\mathrm{R}}(\omega^2 - \omega_0^2)}\phi_{,\alpha} + \frac{G_{\mu\nu|\alpha}}{m_{\mathrm{R}}(\omega^2 - \omega_0^2)}U_{\mu,\nu}. \tag{3.11}$$

The last term on the right-hand side of (3.11) accounts for coupling of relative displacements in optical modes to strains. When inserting (3.11) into (3.4) and (3.6), then solving (3.4) for $\mathbf{U}$ by

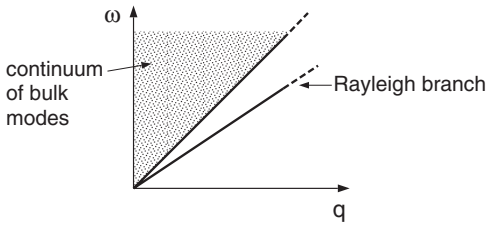

Figure 7. Long-wavelength acoustic part of the phonon dispersion relation of a semi-infinite crystal with elastic isotropy, shown schematically.

iteration and inserting into (3.6), an equation is obtained that contains the electrostatic potential ϕ and its spatial derivatives only. It then becomes clear that the coupling to strains leads to higher derivatives that should be irrelevant for sufficiently slow variations of ϕ. Although these dispersion terms are needed to describe certain modes, we shall neglect them here and obtain an equation for the electrostatic potential with a frequency-dependent dielectric constant (i.e. a dielectric function)

$$\frac{\partial}{\partial X_\alpha}\varepsilon(\omega)\phi_{,\alpha} = 0 \tag{3.12}$$

with the dielectric function

$$\begin{aligned}\varepsilon(\omega) &= \epsilon_\infty - \frac{Z^2}{m_{\mathrm{R}}(\omega^2 - \omega_0^2)} \\ &= \varepsilon_\infty \frac{\omega_{\mathrm{LO}}^2 - \omega^2}{\omega_{\mathrm{TO}}^2 - \omega^2}.\end{aligned} \tag{3.13}$$

At surfaces and interfaces we have to require continuity of the potential and of the normal component of the dielectric displacement field **D**, i.e. of ϕ and of $\varepsilon(\omega)\hat{N}_\alpha\phi_{,\alpha}$.

4. Long-wavelength acoustic modes

On the basis of the set of equations (3.7)–(3.10) and the corresponding boundary conditions we may now investigate various acoustic phonon modes in systems having planar geometries like semi-infinite media, plates and layered structures. If these systems are isotropic in the plane parallel to the surfaces and interfaces (the x–y plane), long-wavelength acoustic modes in these systems may be characterized according to their polarization. They are either polarized in the sagittal plane (the plane spanned by the 2D wavevector and the surface (or interface) normal) or they have shear-horizontal polarization, i.e. the displacements are in the x–y plane orthogonal to the 2D wavevector.

4.1. Modes in a homogeneous semi-infinite crystal

The surface phonon modes with lowest frequency for a given (small) 2D wavevector are normally the Rayleigh modes (figure 7). Their associated displacement field is a linear combination of 3D generalized plane waves, which may be viewed as having a 3D wavevector with real x and y components, but a complex z component. In isotropic media Rayleigh waves consist of two such generalized plane waves. They are polarized in the sagittal plane. The atoms move on ellipses. Their motion is retrograde near the surface and prograde at larger

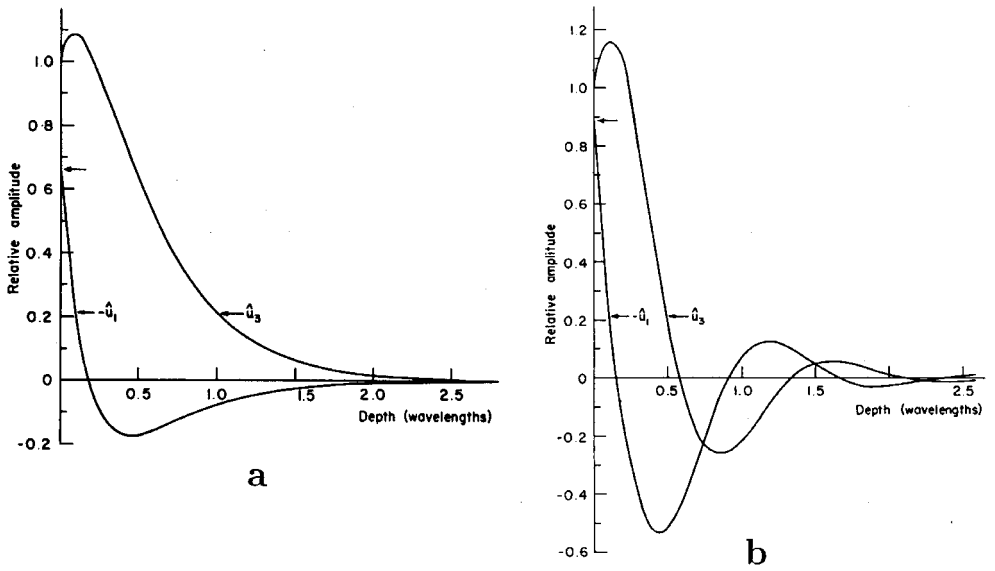

Figure 8. Components of the displacement field parallel ($\hat{u}_1$) and normal ($\hat{u}_3$) to the surface, associated with Rayleigh waves. Isotropic medium (a), Ni(100)⟨001⟩ (b) (from [15]).

depth. The depth profile of the vibrational amplitudes parallel (U_1) and normal (U_3) to the surface is shown in figure 8(a). The penetration depth is of the order of a wavelength.

In anisotropic media, the existence of (generalized) Rayleigh modes is a nontrivial mathematical problem. It has been shown that they exist in almost all geometries (crystal cuts and propagation directions). In non-piezoelectric crystals, their associated displacement field is made up of maximally three generalized plane waves. In piezoelectric media, the number of generalized plane waves is up to four. The decay of the displacement field into depth can have an oscillatory character (figure 8(b)). In the dispersion relation of semi-infinite crystals which are isotropic with respect to their elastic constants, the Rayleigh branch is situated below the continuum of bulk modes. This is the case in many other geometries, too, but not always, as is demonstrated for the (001) surface of nickel in figure 9. When rotating the wavevector from the (100) direction to the (110) direction, the Rayleigh branch comes closer to the band of bulk modes. At the same time, the penetration depth of the Rayleigh mode for fixed wavelength increases. Right at the (110) direction, the Rayleigh mode has become delocalized (i.e. a bulk mode). At the same time, a pure surface mode has appeared with frequencies in the acoustic bulk band. For wavevectors in directions close to the (110) directions, surface resonances appear with frequencies close to those of the new in-band surface mode for given wavelength.

For certain practical applications, for example for the calculation of Brillouin spectra using the matching method [16], long-wavelength normal modes of the semi-infinite crystal have to be determined. In an infinite crystal, these are plane waves ortho-normalized in the usual way. The normal modes of a semi-infinite crystal do not have this simple form because of the broken lattice translational symmetry in the direction normal to the surface. Within continuum theory, normal bulk modes of a semi-infinite crystal may be constructed by letting a plane wave impinge on the surface and add to it the reflected waves. Their presence is required in order to satisfy the boundary conditions for the displacement field at the surface. If, in an isotropic halfspace, the incident wave is of shear-vertical polarization (transverse and polarized in the

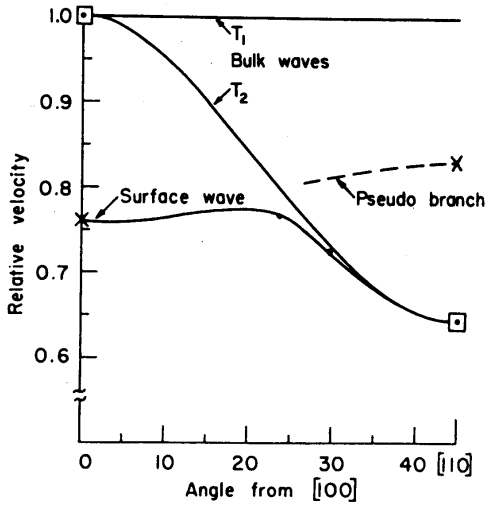

Figure 9. Relative velocities of surface and shear bulk waves at the (001) surface of Ni (from [15]).

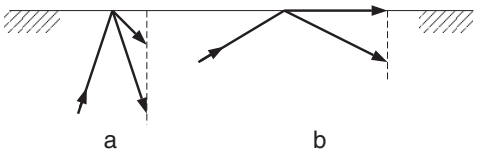

Figure 10. Reflection of an incident shear-vertical plane acoustic wave from a free surface. Two propagating reflected waves (a), one propagating reflected wave and one evanescent wave (b).

sagittal plane), there are two reflected waves for a sufficiently small angle of incidence, one shear-vertical, the other longitudinal (figure 10(a)):

$$\mathbf{U}(\mathbf{X}, t) = \mathrm{e}^{\mathrm{i}(qx-\omega t)}\{\mathbf{A}_{\mathrm{p}1}\mathrm{e}^{\mathrm{i}\kappa_{\mathrm{T}}z} + \mathbf{A}_{\mathrm{p}2}\mathrm{e}^{-\mathrm{i}\kappa_{\mathrm{T}}z} + \mathbf{A}_{\mathrm{p}3}\mathrm{e}^{-\mathrm{i}\kappa_{\mathrm{L}}z}\}, \tag{4.1}$$

where

$$\kappa_{\mathrm{L,T}} = \left[\left(\frac{\omega}{v_{\mathrm{L,T}}}\right)^2 - q^2\right]^{1/2}. \tag{4.2}$$

If the angle of incidence is larger than a critical value, the longitudinal component becomes evanescent and hence is localized exponentially at the surface (figure 10(b)):

$$\mathbf{U}(\mathbf{X}, t) = \mathrm{e}^{\mathrm{i}(qx-\omega t)}\{\mathbf{A}_{\mathrm{p}1}\mathrm{e}^{\mathrm{i}\kappa_{\mathrm{T}}z} + \mathbf{A}_{\mathrm{p}2}\mathrm{e}^{-\mathrm{i}\kappa_{\mathrm{T}}z} + \mathbf{A}_{\mathrm{e}}\mathrm{e}^{\alpha_{\mathrm{L}}z}\}, \tag{4.3}$$

where

$$\alpha_{\mathrm{L}} = \left[q^2 - \left(\frac{\omega}{v_{\mathrm{L}}}\right)^2\right]^{1/2}. \tag{4.4}$$

The velocities of longitudinal and transverse bulk waves in the isotropic medium have been denoted by v_{L} and v_{T}, respectively. The ratios of the amplitudes in (4.1) and (4.3) are determined by the boundary conditions at the surface. The ortho-normalization of the normal modes fixes the absolute values of them. In anisotropic media, the amplitude of the evanescent component of the normal modes, constructed by solving the reflection problem, can be very

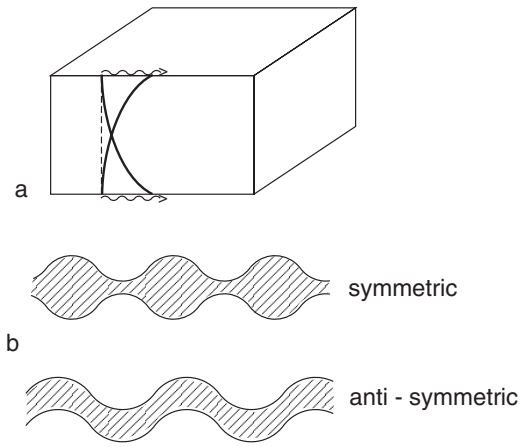

Figure 11. Interaction of Rayleigh modes propagating at the upper and lower surface of a slab (a). Symmetric and anti-symmetric Lamb modes (b).

large in comparison to the amplitudes of the plane waves. Such normal modes correspond to surface resonances.

In addition to these bulk modes, there is the Rayleigh mode which is fully localized at the surface. (For the complete set of long-wavelength acoustic normal modes of an isotropic halfspace see [17].)

In isotropic halfspaces elasticity theory does not allow for a surface mode of shear-horizontal polarization. However, shear-horizontal surface modes exist within electro-elasticity theory in piezoelectric media (Bleustein–Gulyaev modes) [19].

4.2. Modes in structures involving an interface between two media

If the semi-infinite crystal is in contact with another crystal, long-wavelength acoustic modes can appear that are localized at the interface between the two media (Stoneley waves). If the two media are isotropic, these waves are polarized in the sagittal plane. They exist only for certain ranges of material constants of the two media.

If a semi-infinite crystal is covered by a film of a different material, new surface modes exist. In particular, there are now modes of shear-horizontal polarization that decay exponentially into the substrate. In the film, the displacement field oscillates as a function of the coordinate normal to the surface (the z coordinate). There is an infinite number of branches of these Love waves.

In addition to Rayleigh waves, there are other modes of sagittal polarization (generalized Lamb waves or Sezawa waves). Their displacement field in the substrate is evanescent. In the film, it may be oscillatory as a function of Z, evanescent or of mixed character. In the limit of wavelengths much shorter than the thickness of the film, their velocity may converge to the Rayleigh wave velocity of the film material or the Stoneley wave velocity of the interface.

When computing surface modes of a semi-infinite crystal by the method of repeated slabs, a problem occurs in the long-wavelength acoustic limit. With increasing wavelength, the penetration depth of the Rayleigh modes increases, too, and the displacements of the Rayleigh modes localized at the upper and lower surface of a slab overlap (figure 11(a)). This leads to hybridization: the degeneracy of the two Rayleigh branches is lifted, and one obtains the frequencies of plate modes. In the case of sagittal polarization they are called Lamb modes

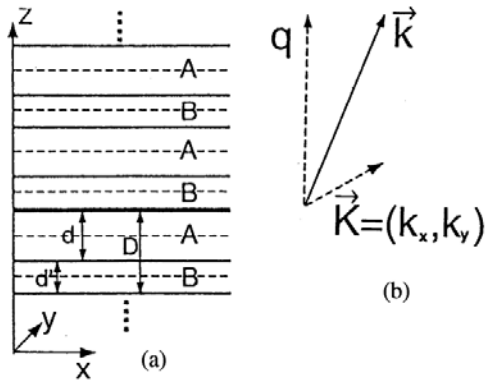

Figure 12. Geometry of an infinite periodic two-component superlattice (a). Decomposition of the 3D wavevector (b).

and can be characterized as symmetric or anti-symmetric (flexural) according to the behaviour of U_3 as a function of z (figure 11(b)). In the limit $q \to 0$ the frequencies of the lowest branch of symmetric Lamb modes behave as $\omega \propto q$, while the frequencies of the lowest branch of anti-symmetric Lamb modes are proportional to q^2 in this limit.

In addition to sagittal plate modes, there are also those of shear-horizontal polarization in isotropic plates (or anisotropic plates with the appropriate symmetry). Interestingly, the lowest branch of the shear-horizontal plate modes is non-dispersive, i.e. the displacement field associated with these modes 'does not feel' the finite extension of the plate along the z axis. For more details on this 'zoo' of long-wavelength acoustic surface modes see, for example, [18, 19].

4.3. Superlattices

Layered structures consisting of a large number of films with different material properties are termed superlattices. The simplest example of such artificial materials is a two-component periodic superlattice, where layers of two different materials are arranged in periodic order (figure 12). The thicknesses of the two types of layers are denoted by d and d' and the thickness of the 'unit cell' of the periodic arrangement by $D = d + d'$. Such structures can be grown by molecular beam epitaxy, for example. If the wavelength of acoustic modes in a superlattice is much larger than the layer thicknesses, the superlattice may be treated as an effectively homogeneous medium with averaged density and elastic moduli. Continuum theory may also be used for modes with wavelengths of the order of D if the layers are sufficiently thick.

For simplicity, we shall assume elastic isotropy of the layers in the plane parallel to the interfaces, i.e. the x–y plane. In this case the acoustic modes may again be grouped into sagittal and shear-horizontal. As a simple example we consider longitudinal or transverse modes propagating normal to the interfaces. In general, the displacement field U ($U = U_3$ for longitudinal and U being a linear combination of U_1 and U_2 for transverse modes) in a medium with material properties varying periodically along the z axis satisfies the equation

$$\rho(z)\ddot{U}(z,t) = \frac{\partial}{\partial z}C(z)\frac{\partial}{\partial z}U(z,t), \tag{4.5}$$

where ρ is the mass density and C is the elastic constant c_{11} for longitudinal and c_{44} for transverse modes. Since ρ and C are periodic functions of z, $\rho(z) = \rho(z + D)$ and $C(z) = C(z + D)$, the Bloch theorem may be invoked which implies that solutions of (4.5)

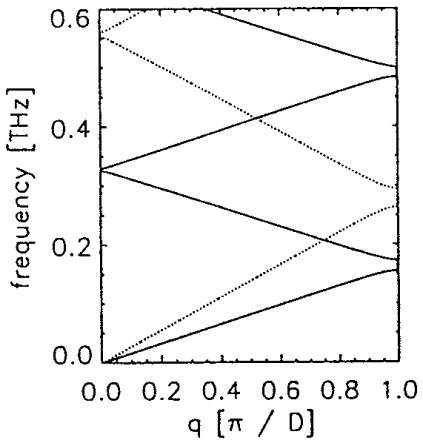

Figure 13. Dispersion curve of acoustic phonons in a GaAs/AlAs superlattice. Wavevector normal to the layers. Transverse (full) and longitudinal (dotted) polarization.

may be found in the form

$$U(z) = \mathrm{e}^{\mathrm{i}qz} w(z), \tag{4.6}$$

where $w(z) = w(z + D)$ and the wavenumber q is restricted to the interval $[-\pi/D, +\pi/D]$, the 'mini-Brillouin zone'. The frequencies of the longitudinal and transverse modes following from (4.5) may be represented as functions of q in the 'mini-Brillouin zone'. If the layers making up the superlattice were identical, the relation between frequency ω and 1D wavevector q in the 'mini-Brillouin zone' would be $\omega = v_{\mathrm{L,T}}(q + n(2\pi/D))$, where $n = 0, \pm 1, \pm 2, \ldots$ and $v_{\mathrm{L,T}}$ is the phase velocity of longitudinal or transverse acoustic bulk waves. This corresponds to a folding of the straight lines $\omega = v_{\mathrm{L,T}} q$ into the 'mini-Brillouin zone'. If density and/or elastic properties of the medium vary periodically, gaps open up at the edges of the 'mini-Brillouin zone' and at its centre (figure 13).

In general, the modes of an infinite periodic superlattice may be labelled by a 3D wavevector $\mathbf{k}$. Its projection on the x–y plane will be called $\mathbf{K}$, while its z component is denoted by q (figure 12(b)). Because of our assumption of elastic isotropy of the single layers, the mode frequencies do not depend on the direction of $\mathbf{K}$. For non-zero $\mathbf{K}$, the longitudinal polarization no longer decouples from the transverse, but in calculating the phonon spectrum, one may still make use of the decoupling of shear-horizontal and sagittal modes. Such calculations are conveniently done by using the transfer matrix technique [20].

The frequencies of the acoustic modes of the superlattice may be represented in the same way as the surface-adapted bulk dispersion relation of a crystal. The frequencies $\omega(\mathbf{k}j)$ are plotted as functions of $\mathbf{K}$ (j is a branch index). In figure 14 such a plot is shown for shear-horizontal modes of a Nb/Cu superlattice [21]. The frequencies of bulk modes appear in bands with gaps between them. On a straight line in the ω–K plane the gaps close. This straight line corresponds to the Brewster angle of shear-horizontal modes in the two-component superlattice.

In a semi-infinite superlattice with a free surface parallel to the layers, modes exist that have displacements localized at the surface. Their frequencies are found in the gaps between the bulk bands.

Figure 15 shows phonon dispersions of sagittal modes for superlattices consisting of layers with large acoustical mismatch (Al/W). Here large gaps are found and the position of the surface branches can depend on which of the two constituent materials forms the top layer [20].

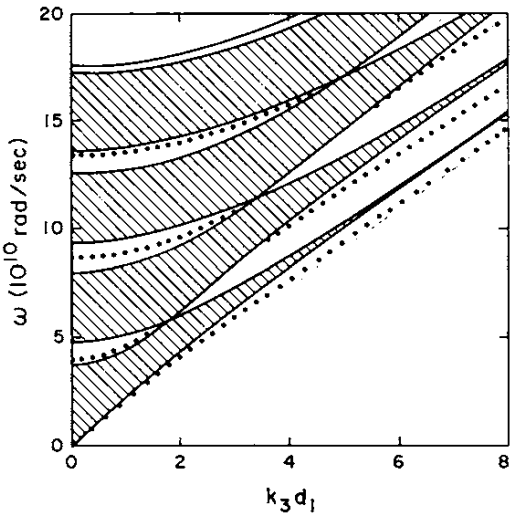

Figure 14. Dispersion relation of acoustic phonon modes of shear-horizontal polarization in a semi-infinite periodic Nb/Cu superlattice (from [21]). $d_{\mathrm{Nb}} = 2d_{\mathrm{Cu}} = 100$ nm. Dotted: surface modes. ($d_1 = d_{\mathrm{Nb}}$ and k_3 corresponds to K in our notation.)

Of practical importance in semiconductor physics are GaAs/AlAs superlattices. The acoustic mismatch between these two materials is comparatively small, and consequently the gaps between the bulk bands are small. The phonon density of states of the superlattice follows almost perfectly a ω^2 law, like the density of states of a homogeneous crystal in the long-wavelength acoustic regime (figure 16). However, numerical calculations reveal small features that occur at frequencies that limit the bulk phonon bands at the centre of the 'mini-Brillouin zone' [22, 23].

Instead of arranging the layers of a two-component superlattice in a periodic order, one may also choose other sequences. This strongly changes the phonon modes. In a random arrangement of layers, all modes are spatially localized apart from special exceptions. Quasi-periodic sequences occupy an intermediate place between periodic and random arrangements of layers. The standard example is the Fibonacci sequence which is generated iteratively. The Nth generation of the superlattice is obtained by appending the $(N-2)$nd generation at the $(N-1)$st generation. If the first generation is a single layer of type B and the second generation a single layer of type A, then the third generation is the double layer AB, the fourth generation the layered system ABA, the fifth the system ABAAB, etc. The phonon spectra of Fibonacci sequences exhibit gaps on all frequency scales. In these gaps, the frequencies of surface localized modes can be found. The penetration depths of these modes are the larger the smaller the gap size. In addition, certain physical quantities associated with the superlattice may exhibit self-similar features. An example is the surface spectral function for shear-horizontal modes:

$$S_{\perp}(K,\omega) = \omega^{-1} \int_{-\infty}^{\infty} \mathrm{d}x \int_{-\infty}^{\infty} \mathrm{d}y \, \mathrm{e}^{\mathrm{i}Kx} D_{22}(x, y, 0; 0, 0, 0|\omega) \tag{4.7}$$

which is relevant for the interpretation of crossed-polarized Brillouin spectra. $D_{\alpha\beta}(x, y, z; x', y', z'|\omega)$ is the elastic Green tensor of the structure and the surface of the superlattice is at $z = 0$. This function and magnifications of certain frequency ranges are shown in figure 17.

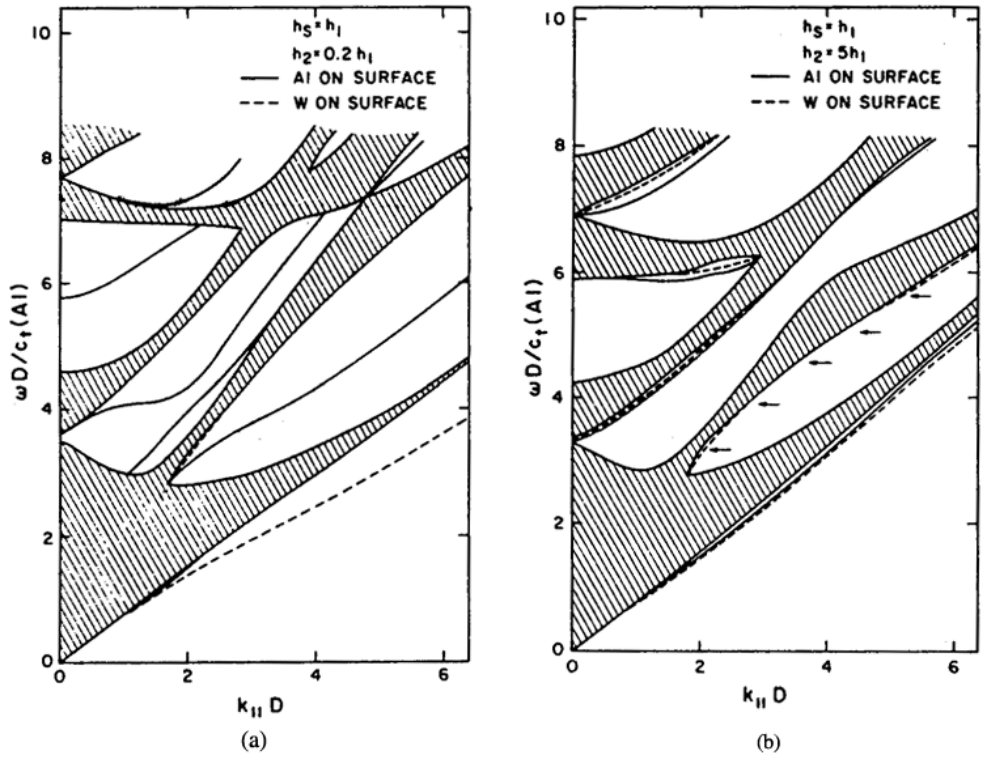

Figure 15. Dispersion relations of acoustic phonon modes of sagittal polarization in a semi-infinite periodic Al/W superlattice (from [20]). $d_{\mathrm{Al}} = 5d_{\mathrm{W}}$ (a), $d_{\mathrm{W}} = 5d_{\mathrm{Al}}$ (b). On the surface, an additional layer of thickness h_{s} has been assumed. ($k_{\parallel}$ corresponds to K in our notation.)

We now return to periodic superlattices and examine their phonon modes on the lattice-dynamical level. Figure 18 shows that the phonon dispersion relation of GaAs/AlAs superlattices in the acoustic regime for wavevectors along the growth direction (the (001) direction) can, to a large extent, be understood by folding the dispersion curves of the pure materials GaAs and AlAs into the new Brillouin zone ('mini-Brillouin zone'). The latter differs from the fcc Brillouin zone of the pure crystals because of the different unit cell of the superstructure that is enlarged in the z direction. The short-hand notation $(\mathrm{GaAs})_n(\mathrm{AlAs})_m$ stands for a periodic superlattice with n monolayers (on the atomic scale) of GaAs following m monolayers of AlAs and vice versa. (To avoid confusion, we would like to stress that the n monolayers of GaAs form one layer of GaAs with the meaning of the word 'layer' previously implied.) The growth direction is (001). The broken curves in figure 18 are the dispersion curves of the pure materials: the upper ones refer to AlAs, the lower ones to GaAs as the Al atoms are lighter than the Ga atoms. (The force constants may be taken to be equal for the two materials to a very good approximation.) At the edge of the 'mini-Brillouin zone', the lowest branch of the superlattice dispersion curve ends approximately at the TA frequency of GaAs at this wavevector. The following branch starts from the 'mini-zone' boundary at the TA frequency of AlAs. The same happens for the next couple of branches and the LA frequencies of GaAs and AlAs.

An interesting feature of GaAs/AlAs superlattices is apparent in figure 18 in the optic regime: the frequency ranges of optical phonons of GaAs and AlAs do not overlap. (The

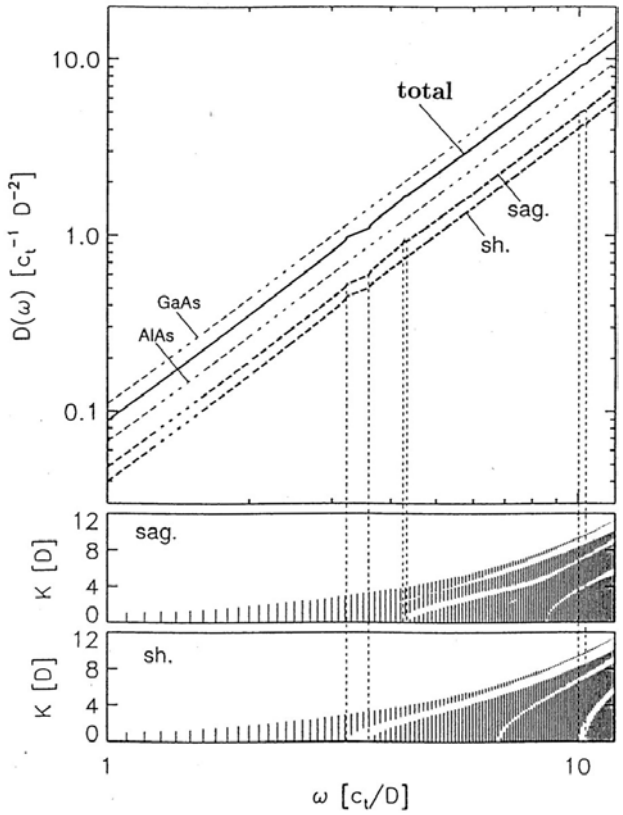

Figure 16. Low-frequency part of the density of states of a periodic GaAs/AlAs superlattice (full curve). For a comparison, the partial densities of states of shear-horizontal and sagittal modes and the phonon densities of states of the homogeneous constituents GaAs and AlAs are shown as broken curves. Lower panels: dispersion relations of sagittal and shear-horizontal modes (from [23]).

highest two broken curves in figures 18(a) and (b) are the LO and TO branches of AlAs, while the following two branches are the LO and TO branches of GaAs.) As a consequence of this fact, the displacements associated with optical modes of the superlattice are confined to one type of layer only ('confined modes'). This is illustrated in figure 19(a), where displacement patterns for two different LO modes of the superlattice are shown with the wavevector at the centre of the Brillouin zone and frequencies in the band of LO modes of GaAs. Corresponding examples for LO modes of the superlattice with frequencies in the LO band of AlAs are shown in figure 19(b).

A satisfactory description of this phenomenon in the framework of continuum theory would require the introduction of dispersion of the optic modes. We shall not pursue this here but discuss macroscopic optical modes for different planar geometries in the following section.

5. Macroscopic optical modes in planar geometries

Macroscopic optical modes localized at the surfaces of semi-infinite crystals or in crystalline plates are called Fuchs–Kliewer modes. To calculate their frequencies for polar diatomic crystals, we may use (3.12) with the form (3.13) of the dielectric function $\varepsilon(\omega)$ and the

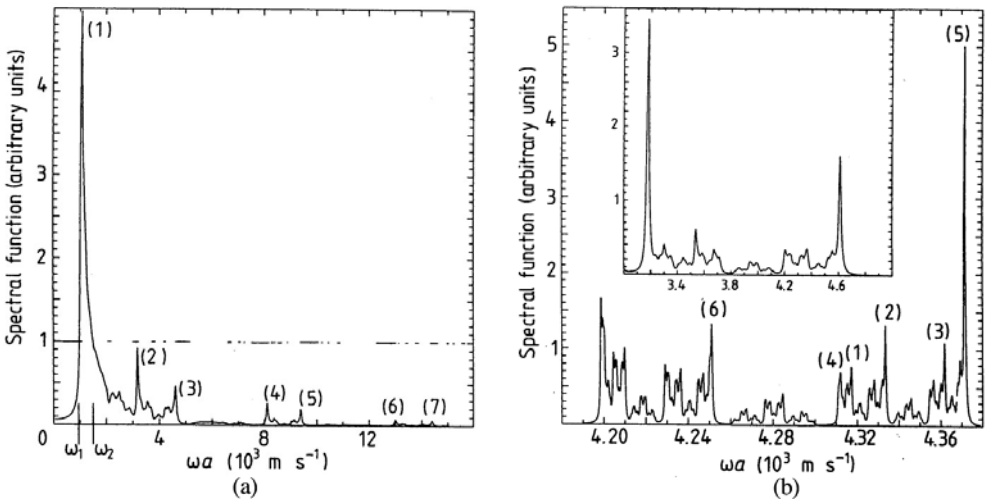

Figure 17. Surface spectral function $S_\perp(K,\omega)$ for a Nb/Cu Fibonacci superlattice, $Kd = 0.5$, $Kd' = 0.25$ (a). Peaks (1)–(7): surface localized modes. The approximate positions of the main gaps are marked by horizontal bars. (b) Magnifications of parts of (a) calculated with higher resolution (from [24]).

corresponding boundary conditions at interfaces, namely the continuity of the electrostatic potential and the normal component of the dielectric displacement field. We first consider the simple case of a semi-infinite crystal filling the halfspace $z < 0$. The ansatz

$$\phi(x,z,t) = \mathrm{e}^{\mathrm{i}(qx-\omega t)\pm|q|z} A_\pm \tag{5.1}$$

for the electrostatic potential in vacuum (lower sign) and in the crystal (upper sign) satisfies the Poisson equation. The boundary conditions at the surface require $A_+ = A_-$ (continuity of ϕ) and $-A_+ = \varepsilon(\omega)A_-$ (continuity of the normal component of **D**). Consequently the frequency ω_{FK} of the macroscopic mode is determined by the equation $\varepsilon(\omega_{\mathrm{FK}}) = -1$. Within the approximation used, ω_{FK} is independent of q, i.e. the mode is non-dispersive and its frequency ω_{FK} is situated between ω_{LO} and ω_{TO}.

This is no longer the case for a crystal plate. Choosing the x–y plane to be the symmetry plane of the plate with thickness $2h$, its surfaces are situated at $z = \pm h$. Similar to the case of acoustic plate modes we expect symmetric and anti-symmetric modes and account for this with the ansatz

$$\phi(x,z,t) = \mathrm{e}^{\mathrm{i}(qx-\omega t)-|q|z} A \tag{5.2}$$

for $z > h$,

$$\phi(x,z,t) = \mathrm{e}^{\mathrm{i}(qx-\omega t)}(\mathrm{e}^{|q|z} \pm \mathrm{e}^{-|q|z})B \tag{5.3}$$

inside the plate, i.e. for $-h < z < h$, and

$$\phi(x,z,t) = \mathrm{e}^{\mathrm{i}(qx-\omega t)+|q|z}(\pm A) \tag{5.4}$$

for $z < -h$. Applying now the boundary conditions at the two surfaces, the following implicit dispersion relations are obtained for symmetric ((5.5), upper sign in (5.2) and (5.4)), and anti-symmetric ((5.6), lower sign in (5.2) and (5.4)) modes:

$$-1 = \varepsilon(\omega)\tanh(qh), \tag{5.5}$$

$$-1 = \varepsilon(\omega)\coth(qh). \tag{5.6}$$

From these relations and the form (3.13) of the dielectric function of the crystal we may deduce

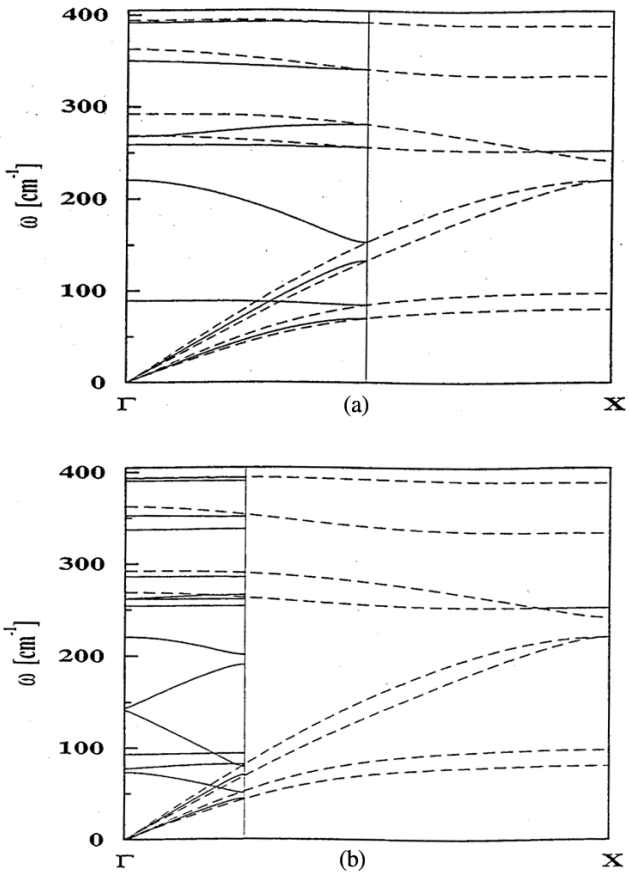

Figure 18. Phonon dispersion curves of short-period GaAs/AlAs superlattices (full) and zone folding of the dispersion curves of pure GaAs and AlAs (broken). $(GaAs)_1(AlAs)_1$ (a), $(GaAs)_2(AlAs)_2$ (b) (from [25]).

that the dispersion curve of symmetric modes approaches ω_{TO} for $q \to 0$ and ω_{FK} for $q \to \infty$. Likewise, the dispersion curve of the anti-symmetric modes tends to ω_{FK} for $q \to \infty$, but it approaches ω_{LO} for $q \to 0$. The above considerations may also be applied and extended to slabs consisting of one material with the two surfaces (or one of them) covered with a film consisting of a different material. As an example, we consider a NaBr slab with both surfaces covered by a LiI monolayer. The continuum treatment now involves four interfaces and two different dielectric functions (figure 20). In figure 21, the results of a lattice dynamical calculation for this system are compared to dispersion curves of macroscopic optical modes obtained in the way described above. The slab consists of 23 layers of NaBr and one monolayer of LiI on both surfaces. The macroscopic modes are clearly distinguishable in the lattice dynamical phonon dispersion relation. One of its branches merges into the band of bulk phonons and hybridizes with the bulk modes. The broken curves in the continuum-theoretical dispersion relation refer to a semi-infinite NaBr crystal covered with one monolayer of LiI. The splitting very close to the centre of the surface Brillouin zone is hence due to the finite thickness of the slab. Similar to the situation for long-wavelength acoustic modes, from a certain wavelength onwards, the slab no longer mimics the dynamical behaviour of a semi-infinite crystal in the frequency regime of optical phonons.

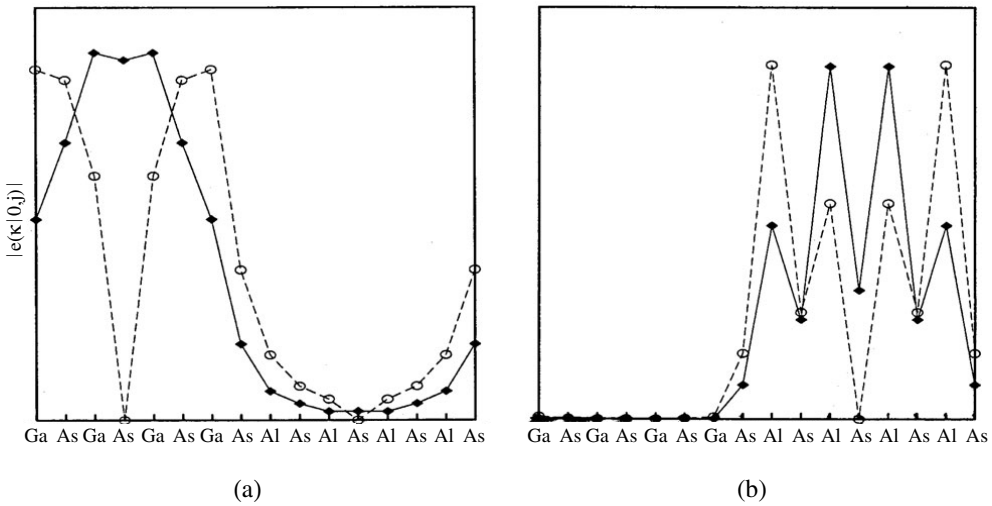

Figure 19. Eigenvectors of 'confined' LO phonon modes of a $(GaAs)_4(AlAs)_4$ superlattice (from [25]). Confinement to GaAs films (a) and to AlAs films (b). The diamonds and open circles represent two different LO modes.

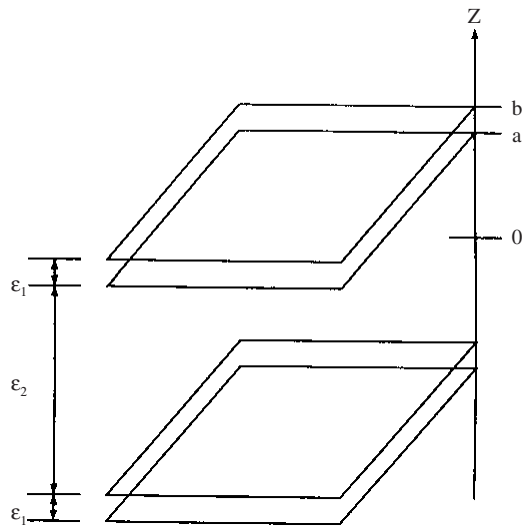

Figure 20. Continuum treatment of a NaBr slab with a LiI film on both surfaces. $\varepsilon_1(\varepsilon_2)$: dielectric function of LiI (NaBr).

In assessing the comparison between lattice and continuum theory, one has to bear in mind that the limits of validity of continuum theory may be somewhat overstretched when applying it to films consisting of one monolayer only.

6. Surface relaxation and reconstruction

We now address lattice effects that are beyond the realm of continuum theory. These are the deviations of the static equilibrium positions of atoms near the surface from the positions

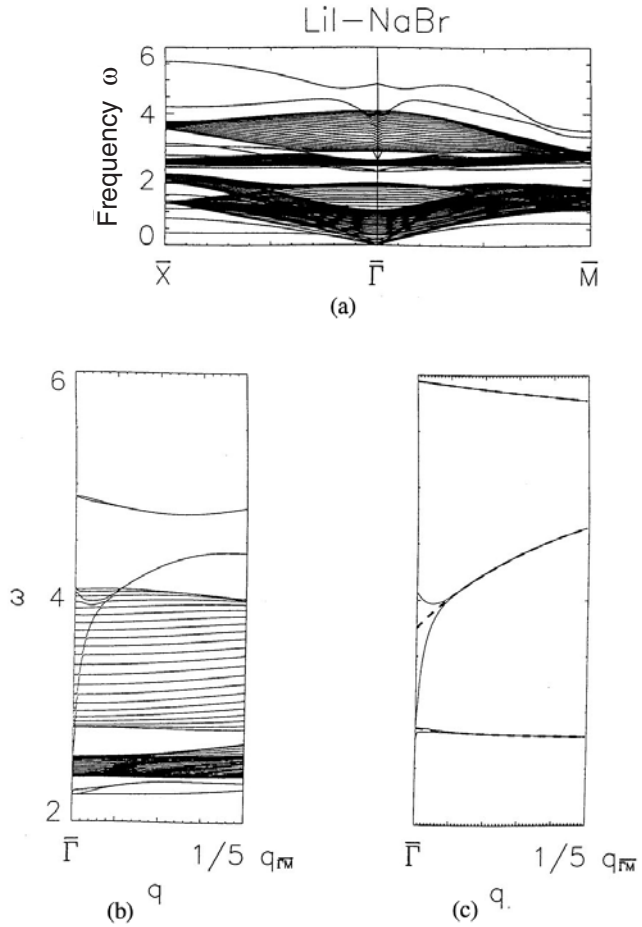

Figure 21. Phonon dispersion relation of a NaBr slab with surfaces covered with one monolayer of LiI. Frequencies in 10^{13} rad s^{-1}. Lattice-dynamical model calculation (a), (b) and results of continuum theory (c) (from [2]).

they would occupy in a bulk crystal. These deviations are caused by the absence of certain bonds at the surface. If the deviations of the positions are minor such that the surface unit cell is not changed from that of the corresponding semi-infinite crystal with all atoms at their bulk equilibrium positions, the phenomenon is called 'relaxation'. If the deviations are extensive, changing the structure near the surface such that the unit cell differs from that of the corresponding semi-infinite crystal with all atoms at their bulk equilibrium positions, we use the term 'surface reconstruction'.

The equilibrium distances of the atoms in a crystal with given structure follow from the equilibrium condition

$$\frac{\partial}{\partial\lambda}\Phi(\{\lambda\mathbf{X}(\ell\kappa)\}) = 0, \tag{6.1}$$

where Φ is the lattice potential. As a simple example we consider a 2D diatomic square lattice with nearest-neighbour and next-nearest-neighbour central potentials $\varphi_{12}(r)$, $\varphi_{11}(r)$,

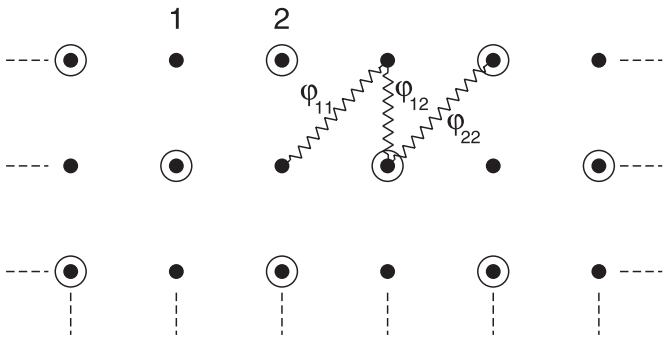

Figure 22. 2D diatomic lattice with nearest-neighbour and second-nearest-neighbour central forces.

and $\varphi_{22}(r)$ (figure 22). The bulk equilibrium condition (6.1) then simplifies to

$$2\varphi'_{12}(r_0) + \sqrt{2}\varphi'_{11}(\sqrt{2}r_0) + \sqrt{2}\varphi'_{22}(\sqrt{2}r_0) = 0, \tag{6.2}$$

where r_0 is the nearest-neighbour equilibrium distance. If the 2D crystal is cut along a straight line, the forces on the surface atoms are normally not zero because of the absence of certain neighbours. In the example of figure 22, these forces can only act normal to the surface because of symmetry. The normal component of the force on surface atoms of type 1 is then

$$F_{\perp}^{(1)} = \varphi'_{12} + \sqrt{2}\varphi'_{11} \tag{6.3}$$

and of type 2

$$F_{\perp}^{(2)} = \varphi'_{12} + \sqrt{2}\varphi'_{22}. \tag{6.4}$$

Because of (6.2), $F_{\perp}^{(1)} = -F_{\perp}^{(2)}$. Consequently the surface atoms of types 1 and 2 are shifted from their bulk equilibrium positions in opposite directions, which leads to a rumpling of the surface.

Even if the relaxation is small, it may have noticeable consequences for the frequencies of certain surface modes. This is illustrated in figure 23, where the phonon dispersion relation of the (001) surface of RbCl is shown in the relaxed and unrelaxed cases. Although the static equilibrium positions of the surface atoms are shifted from their bulk equilibrium positions by less than 0.5%, certain surface phonon branches with associated strong displacements of surface atoms are clearly shifted in the frequency spectrum. This also demonstrates the general fact that the dynamics of a certain lattice system can be used for probing some of its static properties.

A more pronounced type of relaxation occurs on the (110) surfaces of III–V semiconductors having a zincblende structure. The chemical bonds have a predominantly covalent character. The surface relaxation here leads to a tilt angle of about 30°, while the bond lengths are largely unchanged [26] (figure 24).

The surface energy of certain covalently bonded systems can be efficiently reduced by a change of the surface structure, i.e. by reconstruction of the surface. The prototype of an extensive rearrangement of the atoms at the surface is the 7×7 reconstruction of the Si(111) surface. Figure 25 shows the dimer–adatom-stacking fault model for this reconstruction. In this way, the number of dangling bonds can be reduced by a factor of 19/49.

Another surface of silicon, Si(001), is reconstructed by forming dimers. Adsorbed atoms of a different kind can take part in and modify the reconstruction as shown for the B:Si(001)-c(4×4) reconstruction, which involves heterodimers (formed of B–Si pairs) (figure 26).

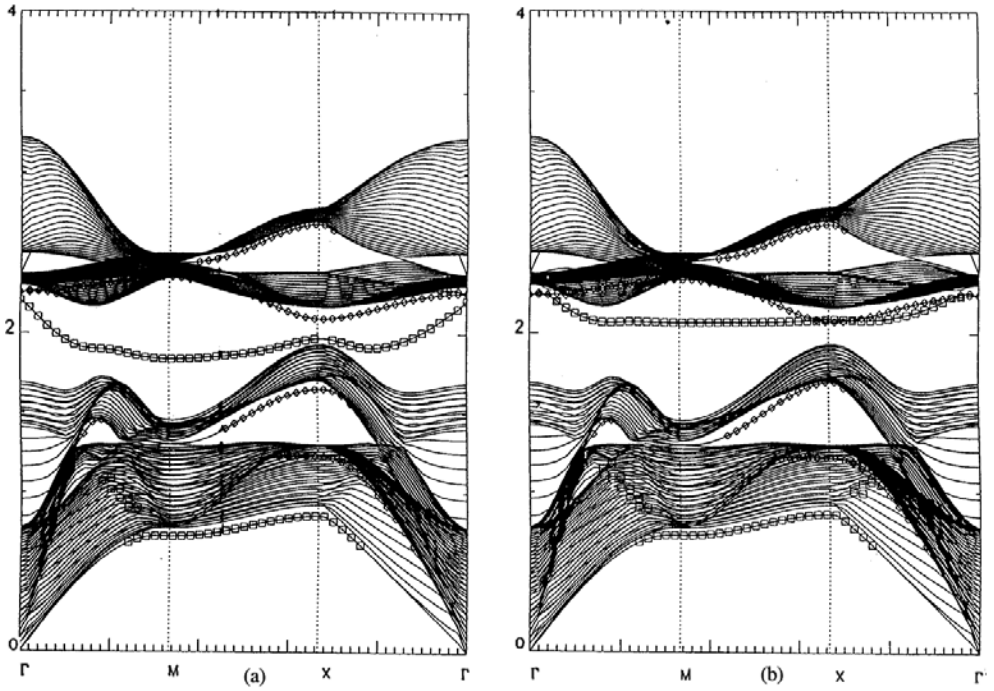

Figure 23. Phonon dispersion relation for the (001) surface of RbCl without surface relaxation (a) and with surface relaxation (b). Surface phonon branches with large displacements normal (parallel) to the surface in the surface layer are marked by squares (diamonds).

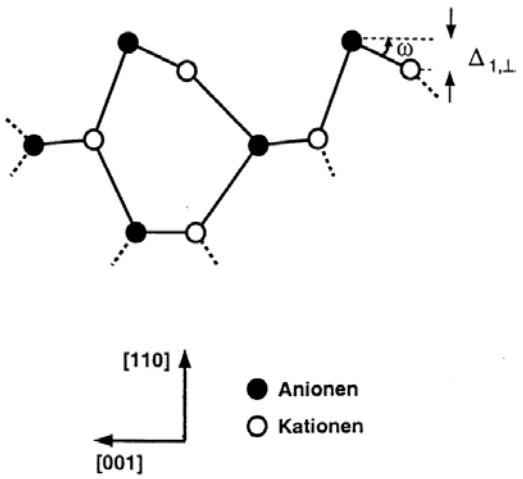

Figure 24. Relaxation of the (110) surfaces of III–V semiconductors (from [26]).

While the pure Si(111) surface strongly reconstructs, this is not the case for the adsorbate systems H:Si(111) and As:Si(111). Here the silicon atoms keep their ideal bulk positions to a good approximation. The hydrogen atoms saturate the dangling bonds and form a triangular lattice on the surface. The As atoms are built into the Si lattice on Si positions (figure 27).

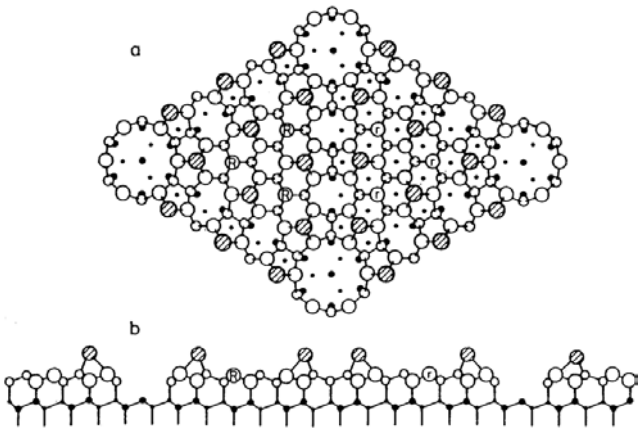

Figure 25. Dimer adatom stacking fault model for the 7×7 reconstruction of the Si(111) surface (from [28] after [27]). For further discussion and references on this reconstruction see [28]. Top view (a), side view (b).

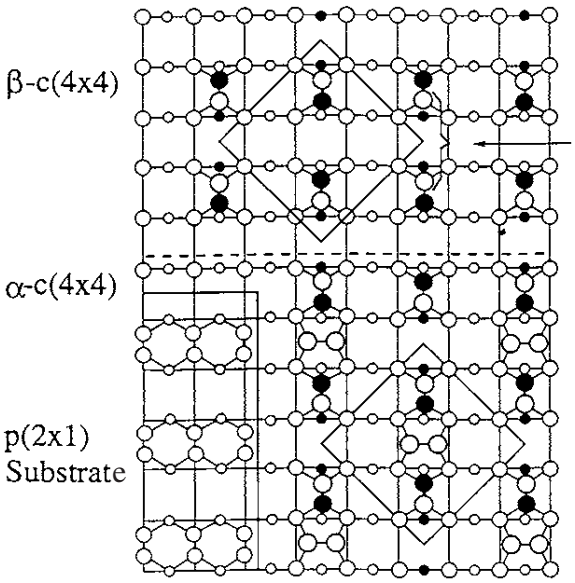

Figure 26. c(4×4) reconstruction of the B:Si(001) surface (from [29]). Open circles: Si atoms in the first (large), second (medium) and third (small) layer. Full circles: B atoms in the first (large) and third (small) layer.

The frequency spectrum of the phonon modes of the adsorbate system H:Si(111) (figure 28) is instructive for the three branches which are located above the highest frequency of the silicon modes. They correspond to modes with associated displacements that involve mostly the adsorbate atoms, namely two hydrogen bending modes which are degenerate at the centre of the surface Brillouin zone, and one stretching mode. It is because of the small mass of the hydrogen in comparison to the silicon atom that these branches are separated from the spectrum of silicon modes.

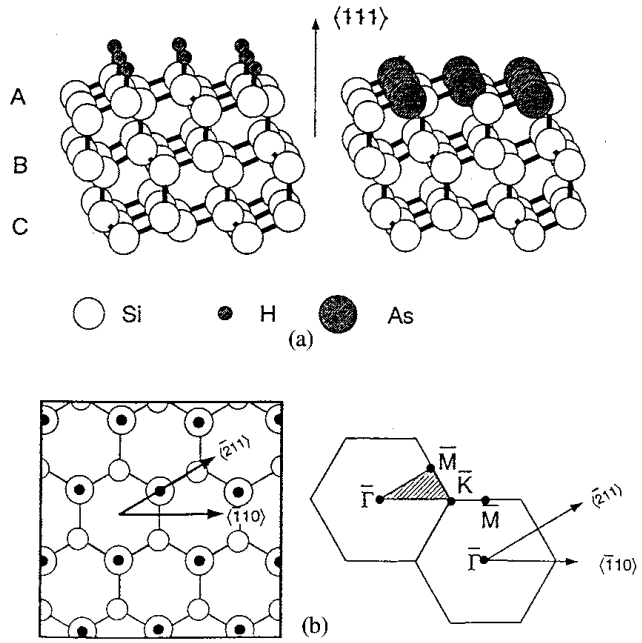

Figure 27. (a) Structure of the H:Si(111) (left) and As:Si(111) (right) adsorbate systems. (b) Top view (left) and surface Brillouin zone (right) of H:Si(111)-(1 × 1) (from [9]).

7. Statics and dynamics of crystal bars

Having discussed systems with planar geometries in the previous sections, we shall now turn to systems with lattice periodicity in only one direction (the z direction), namely crystal bars with quadrangular cross section.

7.1. Relaxation

As examples, we consider bars made out of alkali halides with (100) surfaces. Before analysing the dynamical properties of these systems, we examine their relaxation which is more pronounced than that of infinite (001) surfaces of the same alkali halide, especially at the edges of the bar, leading to a slightly rounded shape (figure 29).

In the relaxation of the bars, two components may be distinguished that can be termed microscopic and macroscopic, respectively. This has been found in model calculations by one of us (DB) [10, 31], who also provided the following explanations for the latter component. He showed that it can be traced back to surface tension and can be understood on the basis of a simple model for a one-atomic simple cubic lattice with nearest-neighbour and second-nearest-neighbour central potentials, denoted by φ_1 and φ_2, respectively (figure 30). (The difference between the two types of atoms in the alkali halide bars is not relevant for the macroscopic part of the relaxation.) The bulk equilibrium condition for this model is

$$\varphi_1'(r_0) + 2\sqrt{2}\varphi_2'(\sqrt{2}r_0) = 0, \tag{7.1}$$

where r_0 is the bulk equilibrium nearest-neighbour distance. This implies that, if the atoms in the bar are situated on bulk equilibrium positions, no force acts on surface atoms that are not at the edges of the bar. (There would be no relaxation of an infinite surface within this

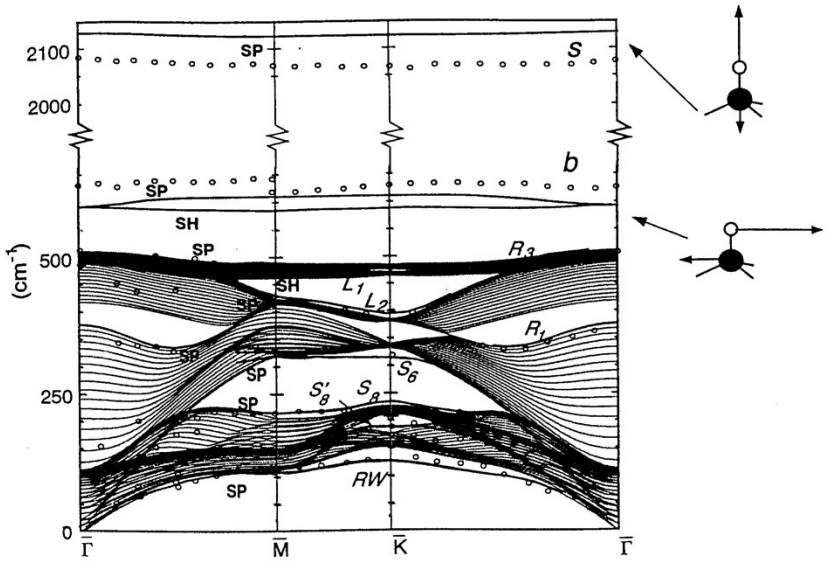

Figure 28. Phonon dispersion relation of H:Si(111)-(1×1). Curves: results of *ab initio* calculations (see [9]), circles: high-resolution electron energy loss spectroscopy data of [30].

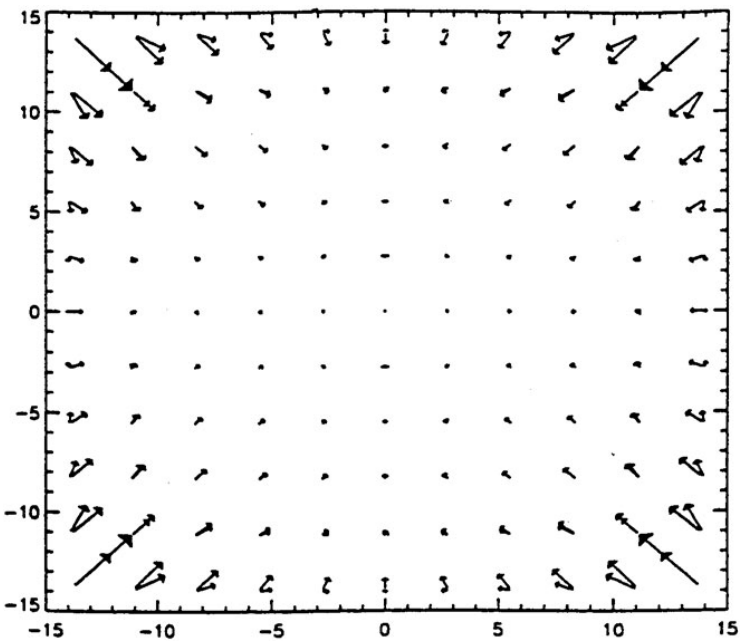

Figure 29. Relaxation of a 11 × 11 bar of NaCl (model calculation). The static displacements are enlarged by a factor of 5 (from [10]). To each position of the unrelaxed lattice, two arrows are attached. One refers to the first and the other to the second layer of the bar's unit cell.

model.) When introducing a cut into the bar along the broken line in figure 30 and breaking the bonds passing through this cut, there will be a force on surface atoms next to this cut, with

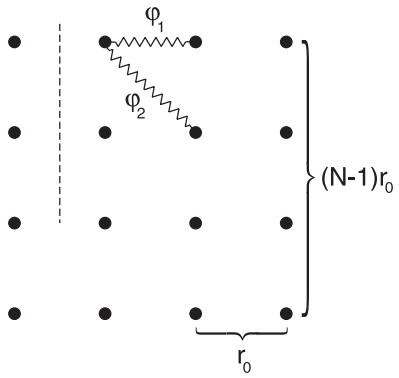

Figure 30. Simple model of a crystal bar with nearest-neighbour and second-nearest-neighbour central forces.

a component parallel to the surface

$$F_{\parallel} = \phi_1' + \frac{3}{\sqrt{2}}\phi_2' = -\frac{1}{\sqrt{2}}\phi_2' \neq 0. \tag{7.2}$$

This means that the surface is under stress and this surface tension has the tendency to contract the bar. To capture this effect in a simple macroscopic description, we replace the surface tension following from (7.2) approximately by a homogeneous pressure p, dividing the force $F_{\parallel}$ by the surface area of a unit cell of the bar:

$$p = \frac{2}{\sqrt{2}}\phi_2'/(Nr_0^2), \tag{7.3}$$

where $N \times N$ is the number of atoms in a cross-sectional layer of the bar. Since N appears in the denominator of the right-hand side of (7.3), the effect of the surface tension plays a lesser role with increasing number of atoms per cross section. The factor of two on the right-hand side of (7.3) is due to the fact that the surface tension of *two* surfaces of the bar leads to a contraction along the x direction.

The homogeneous pressure p leads to an average homogeneous strain $\epsilon = \Delta r/r_0$, where r is the nearest-neighbour distance along the x direction or the y direction, and likewise an average strain $\eta = \Delta r/r_0$, where r is now the nearest-neighbour distance along the z direction. Assuming the pressure $p(\epsilon)$ to be a linear function of ϵ, the equilibrium values of the averaged homogeneous deformations have been determined from the equations of elasticity theory:

$$(c_{11} + c_{12})\epsilon + c_{12}\eta = p(\epsilon), \tag{7.4}$$

$$2c_{12}\epsilon + c_{11}\eta = 2p(\epsilon). \tag{7.5}$$

The factor of two on the right-hand side of (7.5) results from the fact that the surface tension of *four* surfaces instead of two is involved in the contraction along the z direction. Figure 31 shows the behaviour of the average strains ϵ and η as functions of the number N. The symbols are results of microscopic calculations on the basis of simple interatomic potentials, while the curves follow from elasticity theory (equations (7.4) and (7.5)). The full curve and the triangles are obtained when the nearest-neighbour distance along the axis of the bar is fixed to the nearest-neighbour distance of the infinite 3D crystal. The results displayed in figure 31 indicate that the convergence of the average nearest-neighbour distances to their bulk values with increasing number of atoms per cross section is fairly slow.

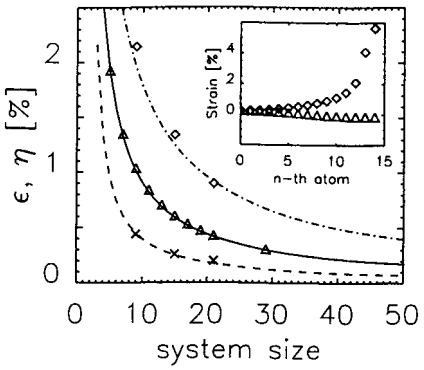

Figure 31. Relaxation of bars with quadrangular cross section, macroscopic component. Symbols: lattice dynamical model calculation, curves: elasticity theory. ϵ (broken and crosses), ϵ with η fixed to 0 (full and triangles), η (chain and diamonds). Inset: strain distribution along the bisectors of the sides (triangles) and the angles (diamonds) of the quandrangular cross section (from [31]).

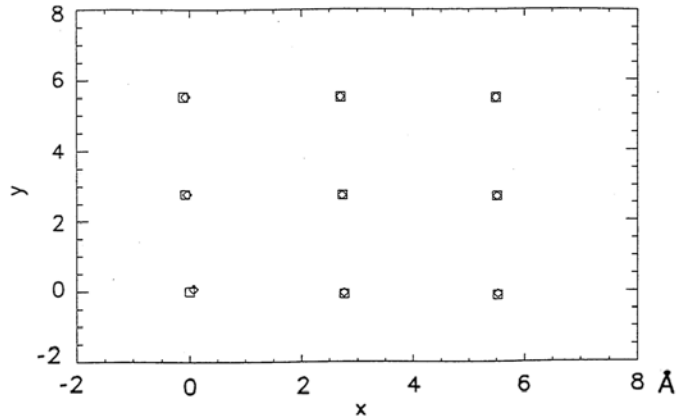

Figure 32. Lower left edge of a 19 × 19 diatomic bar (NaCl). Diamonds: Na ions, squares: Cl ions. (Model calculation, from [10].)

The inset in figure 31 shows the strain distribution in the bar's cross section along the bisector of the sides (triangles) and the bisectors of the angles (diamonds). The quantities ϵ and η can clearly be regarded only as averaged strains. Especially near the edges, the strain distribution is highly inhomogeneous.

In addition to the macroscopic component of the relaxation of diatomic bars, there is a microscopic one that is revealed in figure 32, which shows the lower left corner of the unit cell of a 19 × 19 bar. The rumpling effect discussed already for infinite surfaces (different positions of anions and cations) is particularly pronounced at the edges of the diatomic bar.

7.2. Dynamical properties

A new type of phonon modes in bars as compared to slabs are edge modes. Their associated displacement patterns may be localized to a few atoms in the cross section of the bar, and their frequencies in the dispersion relation appear outside the bands of acoustic bulk modes, optical bulk modes and surface modes of the same irreducible representation of the bar's

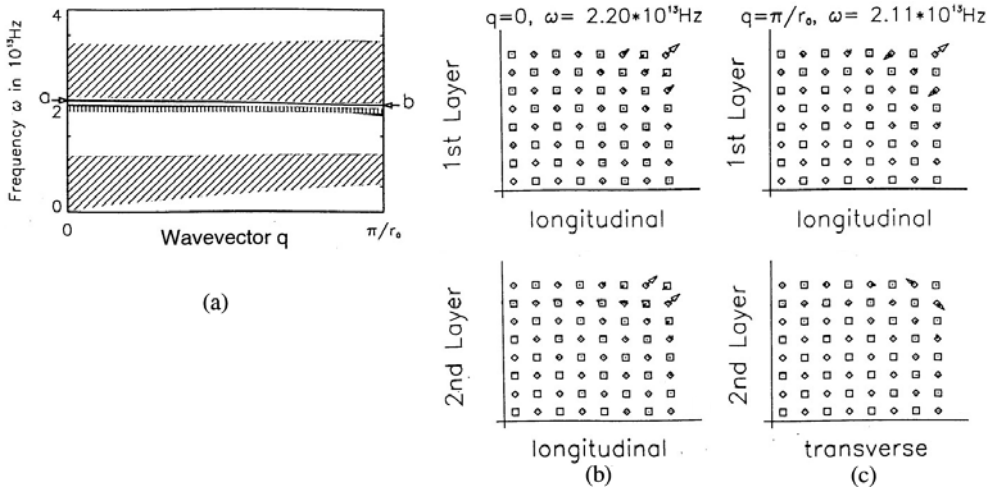

Figure 33. Frequency dispersion of the phonon modes with A1 symmetry of a 15 × 15 diatomic bar (a). The eigenvectors of two edge-localized modes, indicated by 'a' and 'b' in the phonon spectrum, are shown in (b) and (c). (From [31]: for more details see the text.)

symmetry group (C_{4v}). Figure 33(a) shows the dispersion relation of the phonon modes with A1 symmetry in a 15 × 15 diatomic bar. For the displacement patterns of these modes, the two bisectors of the sides and the two bisectors of the edges of the cross section are all mirror planes. In figures 33(b) and (c), the eigenvectors of two highly localized edge modes are shown. The first one has wavevector zero. Its position in the phonon dispersion relation is indicated by 'a' in figure 33(a). It is polarized along the axis of the bar (longitudinal). The z components of the eigenvectors are plotted along a diagonal of the cross section.

The second example is an edge mode with wavevector at the boundary of the 1D Brillouin zone, indicated by 'b' in figure 33(a). In the first layer of the unit cell, it has polarization along the axis of the bar, while the displacements of the second layer are purely transverse (figure 33(c)). Since it is a zone-boundary mode, there is a phase shift between the displacements of the first and second layers.

In the long-wavelength acoustic regime, one may compare lattice-dynamical calculations of phonon modes with the macroscopic modes of a beam following from elasticity theory. There are four modes that have the property $\omega \to 0$ as $q \to 0$. These are:

- one longitudinal mode,
- two bending modes,
- one torsional mode.

While $\omega \propto q$ for the longitudinal and torsional modes, $\omega \propto q^2$ for the bending (flexural) modes. The simple Euler–Bernoulli beam bending theory yields a parabolic dispersion curve which agrees with lattice dynamics for very long wavelengths only. The more sophisticated Timoshenko approach involving two branches yields results in agreement with lattice theory for smaller wavelengths, too.

Relaxation has a dramatic influence on the frequencies of torsional modes [10]. If the bar is not fully relaxed, the frequency of the torsional mode does not tend to zero in the limit $q \to 0$.

The equations of elasticity theory also admit solutions corresponding to waves that propagate along the tip of an infinite wedge [32–34]. For these wedge modes, which are

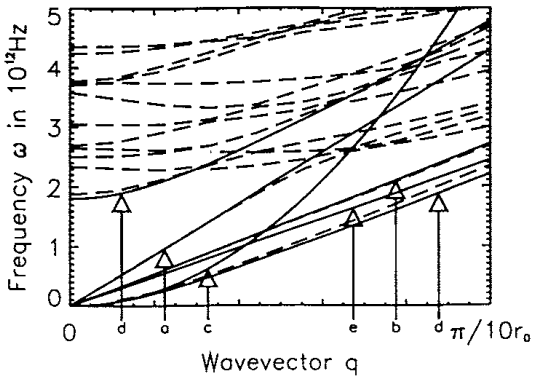

Figure 34. Comparison of macroscopic acoustic modes of a bar (full curves) with lattice-dynamical model calculations for a 15 × 15 bar (broken curves) (from [31]). Longitudinal mode (a), torsional mode (b), flexural mode according to Euler–Bernoulli theory (c), flexural modes according to Timoshenko theory (d), modes localized at the tip of an infinite wedge (e).

of flexural character for the rectangular wedges of the bar investigated here, a quantitative comparison between lattice and continuum theory is difficult. The bar would have to be sufficiently thick that, on the one hand, continuum theory is applicable and, on the other hand, the wedge modes localized at the four edges of the bar do not influence each other. Results of continuum theory are confronted with lattice-dynamical dispersion curves of long-wavelength acoustic modes in figure 34.

The determination of macroscopic optical modes of a bar is not accomplished as easily as for planar geometries and has to be carried out numerically. We briefly describe here an efficient technique for this purpose, which is called the 'source function method' in surface physics and optics or the 'boundary element method' (BEM) in engineering applications (see also [35, 36]). Unlike acoustic wedge modes, there are no macroscopic optic modes localized at the sharp tip of a rectangular wedge and having finite energy content. For this reason and for numerical convenience bars with rounded edges are considered. The cross section of a rounded bar is conveniently described by the inequality

$$0 > \xi_n(x, y) \tag{7.6}$$

with the function $\xi_n(x, y) = x^n + y^n - R^n$. For $n = 2$, we have a circular rod, while in the limit $n \to \infty$ the cross section converges to a square.

The electrostatic potential ϕ in this system may be factorized as

$$\phi(\mathbf{X}, t) = f(\mathbf{r}|q\omega)\mathrm{e}^{\mathrm{i}(qz-\omega t)}, \tag{7.7}$$

where $\mathbf{r} = (x, y)^{\mathrm{T}}$ is the position vector in the x–y plane. From the Poisson equation and the boundary conditions satisfied by ϕ on the surfaces of the bar, the following integral equation may be derived for f with $\mathbf{r}$ on the boundary of the cross section ($\xi_n(\mathbf{r}) = 0$):

$$\frac{1}{1-\varepsilon(\omega)} f(\mathbf{r}|q\omega) = \int_{\xi_n(\mathbf{r}')=0} \mathrm{d}s' H(\mathbf{r}, \mathbf{r}'|q) f(\mathbf{r}'|q\omega), \tag{7.8}$$

where

$$H(\mathbf{r}, \mathbf{r}'|q) = \frac{1}{2\pi} \frac{\partial}{\partial N'} K_0(q|\mathbf{r} - \mathbf{r}'|). \tag{7.9}$$

K_0 is a modified Bessel function and $\partial/\partial N$ denotes the derivative in the direction normal to the boundary of the cross section. Discretizing the contour $\xi_n(\mathbf{r}) = 0$, which is non-trivial

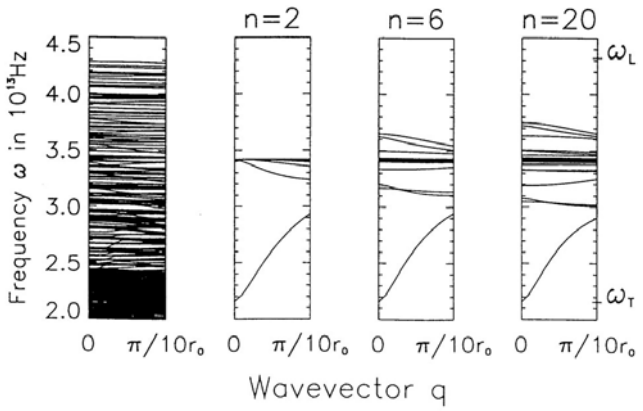

Figure 35. Dispersion relation for optical phonon modes near the Brillouin zone centre for a 15×15 bar (lattice-dynamical model calculation, left panel) in comparison with results of continuum theory for different roundings of the edges (from [31]).

because of the singularity of $H(\mathbf{r}, \mathbf{r}'|q)$, at $\mathbf{r} = \mathbf{r}'$, the integral equation (7.8) is converted into an eigenvalue problem that has to be solved numerically:

$$\frac{1+\varepsilon(\omega)}{1-\varepsilon(\omega)} f(\mathbf{r}_m|q\omega) = \sum_{m'=1}^{M} \mathcal{H}_{mm'}(q) f(\mathbf{r}_{m'}|q\omega), \tag{7.10}$$

where $\mathbf{r}_m, m = 1, \ldots, M$ are discrete points on the boundary of the cross section. The solution of this eigenvalue problem yields the dispersion relation.

In this way frequencies of macroscopic optical modes have been obtained for different roundings of the bar (i.e. different values of n) and compared to lattice-dynamical calculations for a 15 × 15 diatomic bar (figure 35). While the upper part of the spectrum of macroscopic modes strongly depends on the rounding of the bar, the lowest macroscopic optic mode, which is strongly dispersive, is virtually unaffected by the rounding. In the continuum of lattice mode frequencies, traces of this macroscopic mode are visible, hybridizing with the lattice phonon modes.

8. The Jacobi matrix method

Having discussed in some detail phonon modes in systems with lattice translational invariance in two and one dimensions, we shall now briefly introduce a method to calculate lattice dynamical properties without employing a wavevector. In doing this, we follow the presentation given in [38]. This method has recently been applied to clusters adsorbed on a surface and to pyramidal structures on surfaces that form a very simple model for self-organized quantum dots in semiconductor heterostructures [40]. It goes under the names 'Jacobi matrix method', 'continued fraction method' or 'Lanczos method' (see [37, 39] for applications in electronics theory).

For experiments that have local sensitivity to vibrational properties, partial densities of states are a relevant quantity. These are defined as

$$\rho_{\alpha\alpha}(ll|\omega) = \sum_{\lambda} |e_\alpha(l|\lambda)|^2 \delta(\omega - \omega_\lambda). \tag{8.1}$$

Here, l labels the atoms and λ the modes of the system. The contribution of each mode λ in (8.1) is weighted with the modulus square of the eigenvector component $e_\alpha(l|\lambda)$, i.e. with

the square of the modal displacement in the αth Cartesian direction apart from a factor m_l, the mass of atom l. This function can be expressed in terms of the Green function $G_{\alpha\beta}(ll'|\omega)$ of the system, which is the inverse of $\omega^2\delta_{\alpha\beta} - D_{\alpha\beta}(ll')$:

$$\rho_{\alpha\alpha}(ll|\omega) = \frac{\omega}{\mathrm{i}\pi}\{G_{\alpha\alpha}(ll|\omega - \mathrm{i}\epsilon) - G_{\alpha\alpha}(ll|\omega + \mathrm{i}\epsilon)\}. \tag{8.2}$$

$D_{\alpha\beta}(ll') = \Phi_{\alpha\beta}(ll')/\sqrt{m_l m_{l'}}$ is the dynamical matrix.

In order to calculate $G_{\alpha_0\alpha_0}(l_0l_0|\omega)$ for an atom l_0 and direction α_0, one first defines the $3N$-component vector $(V_\alpha^{(0)}(l))$ as $V_\alpha^{(0)}(l) = 1$ if $l = l_0$ and $\alpha = \alpha_0$, and $V_\alpha^{(0)}(l) = 0$ otherwise. (N is the total number of atoms.) Subsequently, a sequence of vectors $\{(V_\alpha^{(n)}(l)), n = 0, 1, \ldots\}$ is generated recursively by applying the dynamical matrix $\mathbf{D}$ to $\mathbf{V}^{(n-1)}$ and orthogonalizing the result to all previous vectors. One finds

$$\mathbf{V}^{(1)} = \mathbf{D}\mathbf{V}^{(0)} - a_0\mathbf{V}^{(0)}, \tag{8.3}$$

$$\mathbf{V}^{(n+1)} = \mathbf{D}\mathbf{V}^{(n)} - a_n\mathbf{V}^{(n)} - b_{n-1}\mathbf{V}^{(n-1)} \tag{8.4}$$

with coefficients a_n and b_n, $n = 0, 1, \ldots$. The vectors $\mathbf{V}^{(n)}$ span a subspace of the configuration space of the system. Within this basis, the dynamical matrix reduced to this subspace is tridiagonal. In order to calculate $G_{00} = G_{\alpha_0\alpha_0}(l_0l_0|\omega)$, one has to determine one element of the inverse of a tridiagonal matrix. This can be done by applying the expansion theorem for determinants. One finds $G_{00} = D_0/D$, where $D = (\omega^2 - a_0)D_0 - b_0D_1$, and the recursion relation $D_n = (\omega^2 - a_{n+1})D_{n+1} - b_{n+1}D_{n+2}$ can be derived. This leads to the continued fraction representation of the desired quantity

$$G_{00}(\omega) = \cfrac{1}{\omega^2 - a_0 - \cfrac{b_0}{\omega^2 - a_1 - \cfrac{b_1}{\omega^2 - a_2 - \cfrac{b_2}{\ddots}}}}. \tag{8.5}$$

The coefficients a_n and b_n converge to limiting values a_∞ and b_∞, which allows for a truncation of the continued fraction by defining

$$r_N(\omega) = \cfrac{1}{\omega^2 - a_{N+1} - \cfrac{b_{N+1}}{\omega^2 - a_{N+2} - \cfrac{b_{N+2}}{\ddots}}}. \tag{8.6}$$

and determining r_N via

$$r_N(\omega) = \frac{1}{\omega^2 - a_\infty - b_\infty r_N(\omega)}. \tag{8.7}$$

In this way, partial densities of states can be calculated efficiently for random systems, and the method has recently been applied to various isolated surface protuberances and adsorbed clusters by the group of AM Kosevich (figure 36). Clearly, reliable force constants have to be known in order to apply this method to real systems.

9. Concluding remarks

It has been our aim to demonstrate that the dynamical behaviour of solid state systems with reduced lattice-translational invariance, as compared to three-dimensional crystals, shows a number of interesting phenomena. Partly, these phenomena can be understood on the basis of continuum theory or with the help of simple lattice-dynamical model considerations. However, in order to achieve a closer insight into such effects and to be able to make quantitative predictions for experiments, much more computational effort has to be invested. Although considerable progress has been made in developing theoretical methods that can cope with systems comprising a large number of atoms in various coordinations, reliable calculations

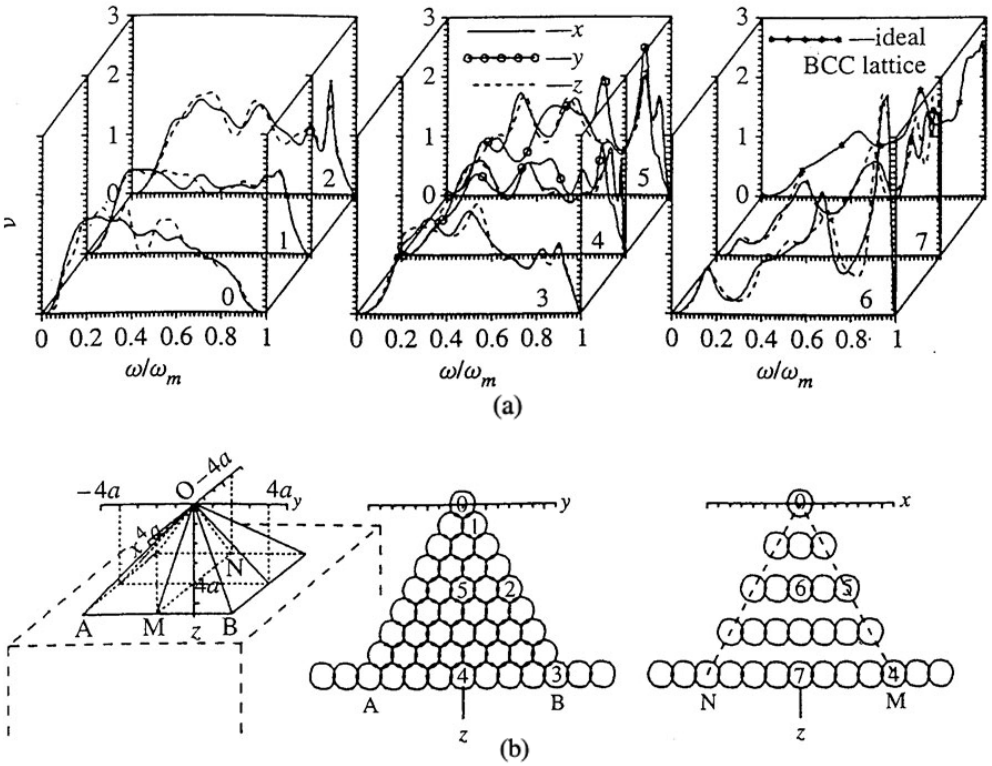

Figure 36. Vibrational partial densities of states for atoms on different sites of a pyramidal cluster (from [40]) (a). Geometry (b).

of frequencies and displacement patterns of vibrational modes in systems with reduced dimensionality are still posing a major challenge. It is worth doing such calculations because, on the one hand, their results yield information about interatomic forces that are not obtainable in bulk materials. On the other hand, they are needed for a detailed quantitative understanding of a number of effects like, for example, heat capacities and thermal conductivities of nanostructures and phonon-assisted electronic processes in composites and nanostructured materials. These are expected to gain increasing technological importance in view of the enormous progress in the fabrication of nanostructured materials seen in recent years.

References

[1] Strauch D, Pavone P, Mayer A P, Karch K, Sterner H, Schmid A, Pletl Th, Bauer R and Schmitt M 1998 *Festkörperprobleme/Advances in Solid State Physics* vol 37, ed R Helbig (Braunschweig: Vieweg) p 99
[2] Bonart D 1996 *PhD Dissertation* University of Regensburg
[3] de Wette F W, Kress W and Schröder U 1985 *Phys. Rev.* B **32** 4143
[4] Sangster M J, Schröder U and Atwood R M 1978 *J. Phys. C: Solid State Phys.* **11** 1523
Sangster M J and Atwood R M 1978 *J. Phys. C: Solid State Phys.* **11** 1541
[5] Goldammer W, Ludwig W, Zierau W and Falter C 1984 *Surf. Sci.* **141** 139
[6] Benedek G and Miglio L 1991 *Surface Phonons* ed W Kress and F W de Wette (Berlin: Springer) p 37
[7] de Wette F W 1991 *Surface Phonons* ed W Kress and F W de Wette (Berlin: Springer) p 67
[8] Fritsch J and Schröder U 1999 *Phys. Rep.* **309** 209
[9] Honke R 1997 *PhD Dissertation* University of Regensburg

[10] Bonart D 1993 *Diploma Dissertation* University of Regensburg
[11] Bonart D, Mayer A P and Schröder U 1995 *Phys. Rev. Lett.* **75** 870
[12] Chen T S, de Wette F W, Kleinman L and Dempsey D G 1978 *Phys. Rev.* B **17** 844
[13] Nelson D F (ed) 1992 *Numerical Data and Functional Relationships in Science and Technology* (*Landolt–Börnstein New Series* vol 29) (Berlin: Springer)
Madelung O, Rössler U and Schulz M (ed) 2001 *Numerical Data and Functional Relationships in Science and Technology* (*Landolt–Börnstein New Series* vol 41) (Berlin: Springer) and earlier volumes of this series
[14] Nelson D F 1979 *Electric, Optic, and Acoustic Interactions in Dielectrics* (New York: Wiley)
[15] Farnell G W 1970 *Physical Acoustics* vol 6, ed W P Mason and R N Thurston (New York: Academic) p 109
[16] Bortolani V, Nizzoli F and Santoro G 1978 *Phys. Rev. Lett.* **41** 31
[17] Ezawa H 1971 *Ann. Phys., NY* **67** 438
[18] Auld B A 1990 *Acoustic Fields and Waves in Solids* 2nd edn (Malabar, FL: Krieger)
[19] Maradudin A A 1985 *Nonequilibrium Phonon Dynamics* ed W E Bron (New York: Plenum) p 395
[20] Djafari-Rouhani B, Dobrzynski L, Hardouin Duparc O, Camley R E and Maradudin A A 1983 *Phys. Rev.* B **28** 1711
[21] Camley R E, Djafari-Rouhani B, Dobrzynski L and Maradudin A A 1983 *Phys. Rev.* B **27** 7318
[22] Tamura S 1997 *Phys. Rev.* B **56** 12440
[23] Schmitt M 1999 *PhD Dissertation* Universit of Regensburg
[24] Mayer A P 1989 *J. Phys.: Condens. Matter* **1** 3301
[25] Steininger B 1996 *Diploma Dissertation* University of Regensburg
[26] Fritsch J and Schröder U 1999 *Phys. Rep.* **309** 209
[27] Takayanagi K, Tanishiro Y, Takahashi M and Takahashi S 1985 *Surf. Sci.* **164** 367
[28] Mönch W 2001 *Semiconductor Surfaces and Interfaces* 3rd edition (Berlin: Springer)
[29] Fritsch J 2000 *Habilitationsschrift* Universität Regensburg
[30] Stuhlmann Ch, Bogdányi G and Ibach H 1992 *Phys. Rev.* B **45** 6787
[31] Bonart D, Mayer A P and Schröder U 1994 *Surf. Sci.* **313** 427
[32] Maradudin A A, Wallis R F, Mills D L and Ballard R L 1972 *Phys. Rev.* B **6** 1106
[33] Lagasse P E 1972 *Electron. Lett.* **8** 372
[34] Moss S L, Maradudin A A and Cunningham S L 1973 *Phys. Rev.* B **8** 2999
[35] Jun Q Lu and Maradudin A A 1990 *Phys. Rev.* B **42** 11159
[36] Knipp P A and Reinecke T L 1992 *Phys. Rev.* B **49** 909
[37] Haydock R 1980 *Solid State Physics* vol 35, ed H Ehrenreich, F Seitz and D Turnbull (New York: Academic) p 215
[38] Maradudin A A 1981 *Modern Problems of Surface Physics* ed I J Lalov (Sofia: Publishing House of the Bulgarian Academy of Sciences) p 11
[39] Fulde P 1995 *Electron Correlations in Molecules and Solids* 3rd enlarged edition (Berlin: Springer)
[40] Kosevich A M, Mayer A, Feodosyev S B, Gospodarev I A, Grishaev V I and Syrkin E S 2000 *Superlattices Microstruct.* **27** 7